T-cell receptor repertoires of tumor-infiltrating lymphocytes after hyperthermia using functionalized magnetite nanoparticles

Aim: Accumulating evidence has indicated that hyperthermia using magnetite nanoparticles induces anti-tumor immunity. This study investigated the diversity of T-cell receptors (TCRs) in tumor-infiltrating lymphocytes after hyperthermia using magnetite nanoparticles. **Materials & methods:** Functionalized magnetite nanoparticles, *N*-propionyl-4-*S*-cysteaminylphenol (NPrCAP)/magnetite, were synthesized by conjugating the melanogenesis substrate NPrCAP with magnetite nanoparticles. NPrCAP/magnetite nanoparticles were injected into B16 melanomas in C57BL/6 mice, which were subjected to an alternating magnetic field for hyperthermia treatment. **Results:** Enlargement of the tumor-draining lymph nodes was observed after hyperthermia. The TCR repertoire was restricted in tumor-infiltrating lymphocytes, and expansion of Vβ11$^+$ T cells was preferentially found. DNA sequences of the third complementarity-determining regions revealed the presence of clonally expanded T cells. **Conclusion:** These results indicate that the T-cell response in B16 melanomas after hyperthermia is dominated by T cells directed toward a limited number of epitopes and that epitope-specific T cells frequently use a restricted TCR repertoire.

Original submitted 14 May 2012; Revised submitted 30 July 2012

KEYWORDS: hyperthermia magnetite nanoparticle melanoma T-cell receptor tumor-infiltrating lymphocyte

Akira Ito*, Masaki Yamaguchi, Noriaki Okamoto, Yuji Sanematsu, Yoshinori Kawabe, Kazumasa Wakamatsu, Shosuke Ito, Hiroyuki Honda, Takeshi Kobayashi, Eiichi Nakayama, Yasuaki Tamura, Masae Okura, Toshiharu Yamashita, Kowichi Jimbow & Masamichi Kamihira

*Author for correspondence: Department of Chemical Engineering, Faculty of Engineering, Kyushu University, 744 Motooka, Nishi-ku, Fukuoka 819-0395, Japan
Tel.: +81 92 802 2753
Fax: +81 92 802 2793
akira@chem-eng.kyushu-u.ac.jp
For a full list of affiliations please see the back page

Hyperthermia is a promising approach to treat a wide variety of tumors in patients [1,2]. A major technical problem with currently available clinical hyperthermia systems, including whole-body hyperthermia [3] and local hyperthermia by radiofrequency [4], is the difficulty of heating the tumor region to the intended temperature without damaging normal tissue. Increasing temperatures above 42.5°C can kill greater numbers of tumor cells, but normal tissues are also damaged by these conventional hyperthermia systems. Therefore, the development of a tumor-targeted hyperthermia system is required. Current developments in nanotechnology have made it possible to use a nanometric heat mediator that can generate heat under an external alternating magnetic field (AMF) [5]. Magnetite (Fe_3O_4) nanoparticle-mediated hyperthermia has been a largely experimental modality that has the potential to overcome the shortcomings of conventional hyperthermia systems [6,7]. The technique involves targeting nanoparticles to tumor tissue, and then applying an AMF to induce heat generation by hysteresis loss or relaxation loss [7,8]. In recent years, remarkable advances have been seen in magnetite nanoparticle-mediated hyperthermia for both tumor-targeted magnetite nanoparticles [9,10] and AMF generators [11,12], and some of these techniques have entered clinical trials [13].

By specifically delivering the magnetite nanoparticles to the tumor site, tumor-targeted hyperthermia can be created [14–16]. Melanogenesis uniquely occurs in melanocytic cells. Thus, tyrosine analogs that are tyrosinase substitutes are good candidates for melanoma-specific targeting. The melanogenesis substrate, *N*-propionyl-4-*S*-cysteaminylphenol (NPrCAP), is selectively incorporated into melanoma cells [17]. Based upon the unique biological properties of NPrCAP, the authors have established a novel nanomedicine for melanoma by conjugating NPrCAP to the surface of magnetite nanoparticles to produce NPrCAP/magnetite (NPrCAP/M), which is selectively incorporated into melanoma cells and generates heat upon exposure to AMF [18]. When mice bearing B16F1 melanoma were intraperitoneally injected with NPrCAP/M, the nanoparticles were delivered to the melanoma in the subcutis through the bloodstream [18]. However, a large part of NPrCAP/M was captured in reticuloendothelial cell systems, such as the liver and spleen, in the mice. Therefore, clinical trials using the present nanoparticles may be limited to lesional therapy against melanoma. Current methods

Future Medicine part of fsg

of delivering magnetite nanoparticles in clinical hyperthermia depend on direct injection of the functionalized magnetite nanoparticles into the tumor site [15,19]. Although the procedure is practical for easily accessible tumors including melanoma, this direct injection may limit the usefulness of magnetite nanoparticle-mediated hyperthermia for systemically metastatic melanomas. On the other hand, we have shown that heat treatment also induces anti-tumor immunity by enhancement of heat-shock protein expression [20,21]. Previously, the authors showed that hyperthermia using NPrCAP/M elicited a cytotoxic T-lymphocyte (CTL) response via the release of heat shock protein–peptide complex from degraded tumor cells [22]. Thus, even local magnetic hyperthermia could induce a form of vaccination against tumor cells and may be effective not only for primary melanoma but also for distant metastases.

$CD8^+$ CTLs play a significant role in antigen-specific immune responses to tumors. In our previous study, $CD8^+$ T cells were observed within B16 melanomas after hyperthermia using NPrCAP/M [23]. Clinically, the presence of tumor-infiltrating lymphocytes (TILs) has been considered to be a favorable prognostic indicator [24]. In general, T cells isolated from tumor-draining lymph nodes (DLNs) have also been used as a source of TILs, because these lymph nodes directly drain the tumor. TIL reactivity to antigen is mediated via T-cell receptors (TCRs) comprising α and β chains. The β chain is composed of variable (V), diversity (D), joining (J) and constant regions. TCR diversity is produced by the random insertion or deletion of nucleotides at the V(D)J junctions. The V(D)J junctions code for the putative third complementarity-determining region (CDR3), which is thought to play the most important role in antigen recognition [25]. The TCR repertoire of a T-cell population is thus defined by its different V(D)J gene usage, as well as by the CDR3 characteristics. In the present study, the TCR repertoire after hyperthermia using NPrCAP/M was studied to further understand the T-cell response to melanoma after hyperthermia using NPrCAP/M and to develop more effective cancer immunotherapy based on magnetite nanoparticle-mediated hyperthermia.

Materials & methods

Preparation of NPrCAP/M

The magnetite nanoparticles (average particle size: 10 nm) were purchased from Toda Kogyo (Hiroshima, Japan). Magnetic characterizations of the magnetite at 796 kA/m (at room temperature) were 2.0 kA/m, 63.9 Am^2/kg and 2.6 Am^2/kg for coercivity, saturation flux density and remanent flux density, respectively. The preparation of NPrCAP/M is described elsewhere [18]. Briefly, magnetite nanoparticles were coated with aminosilane and conjugated with NPrCAP via maleimide crosslinkers. The resultant NPrCAP/M were suspended in H_2O to a concentration of 40 mg/ml. Average particle size of NPrCAP/M was approximately 280 nm. The specific absorption rate value was 42.6 W/g at 118 kHz and 30.6 kA/m (384 Oe). The amount of NPrCAP incorporated with magnetite nanoparticles was approximately 60 nmol/mg as determined by hydrolysis with 6 M HCl followed by HPLC analysis of the released 4-*S*-CAP.

Cell culture & establishment of tumors in mice

Mouse B16F1 melanoma cells (American Type Culture Collection, VA, USA) were cultured in DMEM (Gibco BRL, MD, USA), supplemented with 5% fetal calf serum, 0.1 mg/ml streptomycin sulfate and 100 U/ml potassium penicillin G. Cells were grown at 37°C in a humidified atmosphere of 5% CO_2 and 95% air.

All animal experiments were approved by the Ethics Committee for Animal Experiments of the Faculty of Engineering, Kyushu University (A22-180-0). To prepare tumor-bearing mice, cell suspensions containing 5×10^5 B16F1 cells in 50 µl of phosphate-buffered saline were injected subcutaneously into the right hind foot pad of C57BL/6 mice (age: 4 weeks; Japan SLC, Hamamatsu, Japan) after anesthesia by intraperitoneal injection of pentobarbital (50 mg /kg bodyweight) on day 1.

Hyperthermia using NPrCAP/M

NPrCAP/M (50 µl; net magnetite amount: 2 mg) were injected subcutaneously into the melanoma nodule on days 3, 5 and 7. An AMF was generated using a horizontal coil (inner diameter: 7 cm; length: 7 cm) with a transistor (Dai-ichi High Frequency, Tokyo, Japan). The magnetic field frequency and intensity were 118 kHz and 30.6 kA/m (386 Oe), respectively. After the administration of NPrCAP/M, anesthetized mice were placed in the inverter coil with their foot at the center and were exposed to the AMF inside the coil for 30 min on days 3, 5 and 7. Temperatures at the tumor surface and in the rectum were measured using an optical

fiber probe (Anritsu Meter, Tokyo, Japan). The therapeutic temperature was controlled at 43°C by measuring the tumor temperature and adjusting the power of the transistor inverter throughout the AMF exposure.

The tumor was resected and weighed 2 weeks after the first treatment (on day 17). For immunohistochemical examination, tumor tissues were immediately frozen in optimal cutting temperature compound (Sakura Finetechnical, Tokyo, Japan). Thin slices (4 μm) of the frozen tumor tissues were incubated at 37°C for 60 min with rat monoclonal antibody against mouse CD8a (clone: 53-6.7, BD Pharmingen, CA, USA). These sections were subsequently incubated at 37°C for 30 min with biotinylated anti-rat IgG (Dako, Glostrup, Denmark). Specimens were incubated at 37°C for 30 min with peroxidase-conjugated streptavidin (Dako). Each step was followed by washing with Tris-buffered saline. Peroxidase activity was visualized by diaminobenzidine tetrahydrochloride–nickel solution containing 0.007% hydrogen peroxide. Slides were counterstained with methyl green. For negative controls, primary antibodies were replaced with an unrelated IgG.

Isolation of CD8$^+$ TILs & flow cytometric analysis

Mice were anesthetized and lymph nodes were resected to isolate CD8$^+$ T cells 2 weeks after the first hyperthermia treatment (on day 17). For lymph node mapping, 1% Evans blue dye (Sigma-Aldrich, MO, USA) in 25 μl Hank's buffered salt solution [26] was subcutaneously injected into the hind foot pad. The blue-labeled inguinal lymph node from the tumor side of the mouse was taken as the tumor DLN, and the contralateral inguinal lymph node was considered to be a non-DLN [27]. The diameter of lymph nodes was measured using calipers, and the size was determined by applying Equation 1:

$$\text{Lymph node volume} = 0.5\,(\text{length} \times \text{width}^2) \quad (1)$$

Single-cell suspensions of lymph nodes were prepared using the gentleMACS™ Dissociator (Miltenyi Biotec, Bergisch Gladbach, Germany). The CD8$^+$ T cells were isolated from the cell suspension by collection with CD8a (Ly-2) MicroBeads® using a MACS® MS separation column according to the manufacturer's instructions (Miltenyi Biotec). Naive mice that were born at nearly the same time were used as controls. For flow cytometric analysis of CD8, the CD8$^+$ T cells were isolated from the cell suspension by negative selection using a CD8a$^+$ T-cell Isolation kit and a MACS MS separation column according to the manufacturer's instructions (Miltenyi Biotec). For single staining of CD8, the cells that were obtained from the negative selection were mixed and stained with phycoerythrin-conjugated anti-CD8 antibody (CD8a–phycoerythrin, Miltenyi Biotec). For double staining of CD8 and TCR Vβ11, the negatively selected cells were mixed and stained with both peridinin chlorophyll protein-conjugated anti-CD8 antibody (CD8–peridinin chlorophyll protein, Miltenyi Biotec) and fluorescein isothiocyanate-conjugated anti-TCR Vβ11 (clone RR3-15; BD Pharmingen). Flow cytometric analyses were performed to analyze the percentage of CD8$^+$ or CD8$^+$/TCR Vβ11$^+$ T cells using a FACSCalibur™ Flow Cytometer (BD Bioscience, NJ, USA). The number of CD8$^+$ T cells in a lymph node was calculated from the percentage of CD8$^+$ T cells in the total number of lymphocytes that were counted by the trypan blue dye exclusion method using a hemocytometer.

Reverse-transcription PCR & DNA sequencing

Expression of TCR Vβ repertoires was assessed using the SuperTCRExpress™ Mouse T Cell Receptor Vβ Repertoire Clonality Detecting Kit according to the manufacturer's protocol (BioMed Immunotech, FL, USA). This assay system comprises V(D)Jβ-specific PCR amplifications and a gel-based assay. In brief, total RNA was extracted from the CD8$^+$ T cells isolated from a lymph node or the melanoma nodule resected 2 weeks after the first hyperthermia treatment (on day 17). cDNA was synthesized from the isolated RNA, and *TCR* genes were amplified in a single step of 35 PCR cycles. A nested PCR amplified specific *TCR* genes using *TCR Vβ* gene-specific oligonucleotides after an additional 30 cycles. PCR products were resolved on a 4% high-resolution agarose gel. Clonality and diversity in the CDR3 region of the *TCR Vβ* repertoire in mouse T lymphocytes could be confirmed by examination of the *TCR Vβ* expression pattern [28]. For DNA sequencing, TCR Vβ-chain bands on a gel were cut out and purified using the MagExtractor™-PCR & Gel Clean Up Kit (Toyobo, Osaka, Japan). The amplified PCR products were cloned into the pGEM®-T vector (Promega, WI, USA). Plasmid DNA from positive colonies was sequenced using a DNA sequencer (Prism® 3130 Genetic

doi:10.2217/NNM.12.142

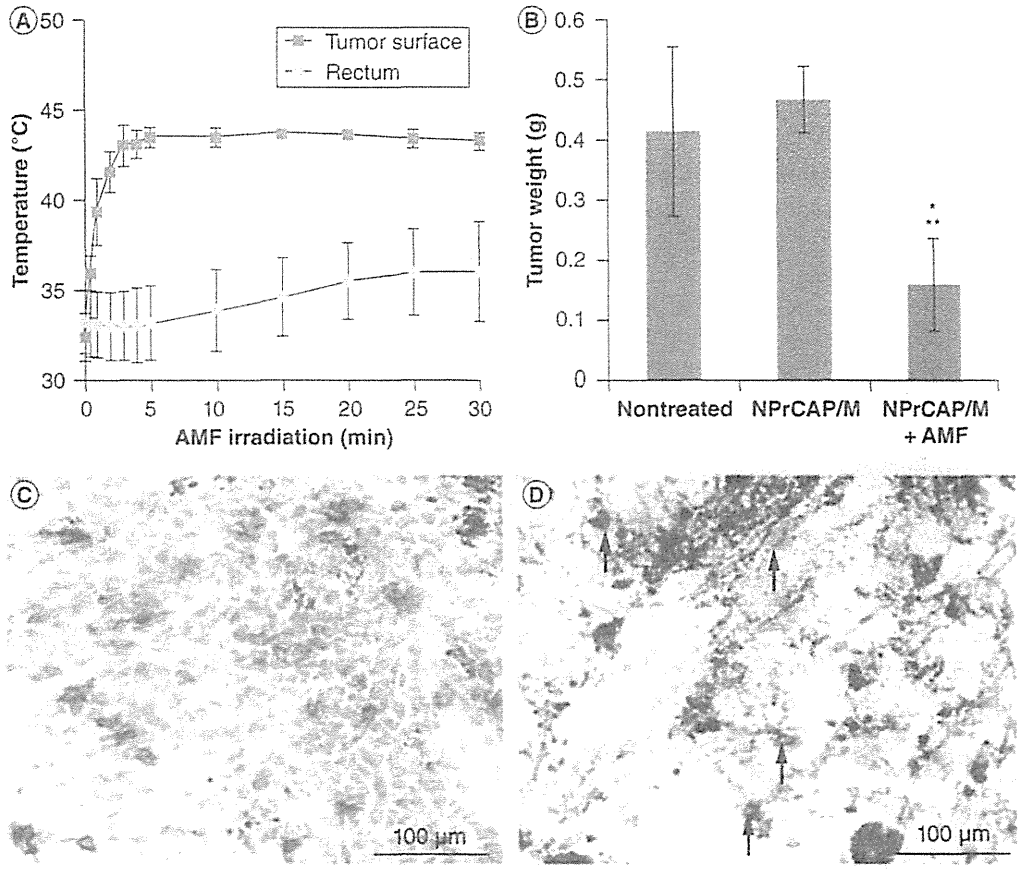

Figure 1. Hyperthermia using *N*-propionyl-4-*S*-cysteaminylphenol/magnetite.
(A) Temperatures at the tumor surface (squares) and in the rectum (circles) during AMF irradiation. NPrCAP/M were injected directly into subcutaneous B16 tumors. Data points and bars are the means and standard deviations from five mice. **(B)** Tumor weight on day 17. Untreated tumors or those injected with NPrCAP/M with or without AMF irradiation were resected, and tumor weight was measured on day 17. Data are the means and standard deviations from five mice. **(C & D)** Immunohistochemical staining for $CD8^+$ T cells **(C)** around and **(D)** within the tumor on day 17. Tumors were resected after NPrCAP/M-mediated hyperthermia. Violet-blue cells are anti-CD8 antibody-stained cells visualized by diaminobenzidine tetrahydrochloride–nickel solution containing hydrogen peroxide. Slides were counterstained with methyl green, and nuclei are light green. Arrows in **(D)** show a few representative $CD8^+$ T cells within the tumor.
*$p < 0.01$ against untreated mice.
**$p < 0.01$ against the mice treated with NPrCAP/M alone.
AMF: Alternating magnetic field; NPrCAP/M: *N*-propionyl-4-*S*-cysteaminylphenol/magnetite.

Analyzer; Applied Biosystems, CA, USA), and the sequences were compared to the GenBank database using the BLAST search engine.

Assay of amounts of IFN-γ in culture supernatants

After the hyperthermia treatment, DLNs from five mice were harvested on day 17, and lymphocytes were then restimulated *in vitro* with mitomycin C-treated B16F1 cells (1×10^5 cells) or antigen peptides (10 µg/ml) in 10 ml of RPMI-1640 supplemented with 50 µM of β-mercaptoethanol and 10% fetal calf serum for 5 days. For the restimulation, B16F1 cells were pretreated with IFN-γ (100 units/ml) for 48 h because B16 cells express MHC class I molecules at a low level, which can be enhanced by IFN-γ treatment [29]. The melanoma-associated antigen peptides used in this study were tyrosinase-related protein (TRP)-$1_{222-229}$ (amino acid sequence: TWHRYHLL; synthesized by Greiner Bio-One, Frickenhausen, Germany) [30], TRP-$2_{180-188}$ (amino acid sequence: SVYDFFVWL; Abgent, CA, USA) [31], and glycoprotein 100_{25-33} (amino acid sequence: EGSRNQDWL; AnaSpec, CA, USA) [32]. As a negative control, ovalbumin peptide ($OVA_{257-264}$; amino acid sequence: SIINFEKL peptide; Abbiotec, CA, USA) was used [33]. Purity of these peptides was >90%. After

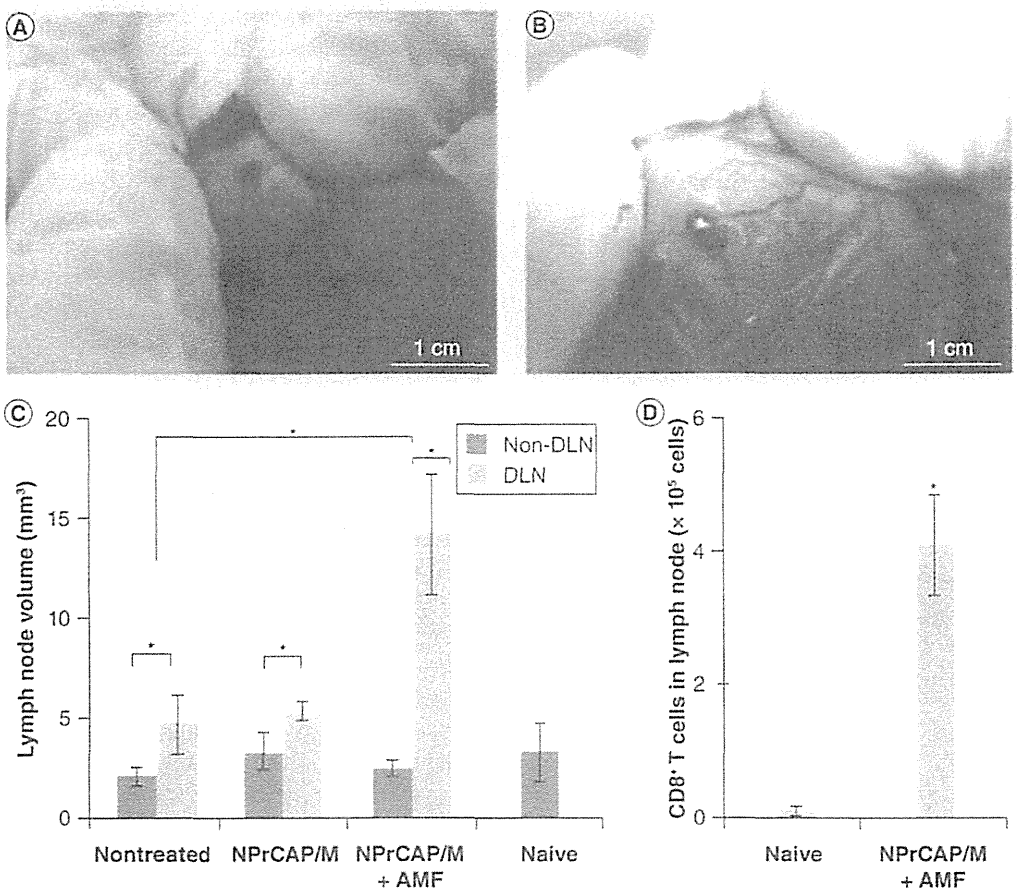

Figure 2. Analysis of lymph node after *N*-propionyl-4-*S*-cysteaminylphenol/magnetite-mediated hyperthermia. (A & B) Evans blue dye labeling of a representative inguinal **(A)** non-DLN and **(B)** DLN. On day 17, 1% Evans blue dye solution was subcutaneously injected into the hind foot pad. **(C)** Lymph node volume on day 17. Data are the means and standard deviations from five mice. **(D)** The number of $CD8^+$ T cells in a lymph node on day 17. $CD8^+$ T cells were negatively selected by magnetic cell sorting. The cells were mixed and stained with phycoerythrin-conjugated anti-CD8 antibody, and flow cytometric analyses were performed to analyze the percentage of $CD8^+$ T cells. The number of $CD8^+$ T cells in a lymph node was calculated from the percentage of $CD8^+$ T cells among the total number of lymphocytes that were counted by the trypan blue dye exclusion method using a hemocytometer. Data are the means and standard deviations from five mice.
*$p < 0.01$.
AMF: Alternating magnetic field; DLN: Draining lymph node; NPrCAP/M: *N*-propionyl-4-*S*-cysteaminylphenol/magnetite.

the restimulation, culture supernatants were collected and amounts of IFN-γ were measured by sandwich ELISA (Thermo Fisher Scientific, IL, USA) according to the manufacturer's instructions. Data were presented as picograms of IFN-γ per milliliter.

Statistical analysis

Statistical analysis was performed by the Mann–Whitney rank sum test calculated using WinSTAT statistical software (Light Stone International, Tokyo, Japan). Differences were considered to be statistically significant at $p < 0.05$.

Results & discussion

Hyperthermia by means of NPrCAP/M

For superficial melanoma, a simple heat mediator is desirable for clinical application. We previously showed the therapeutic effects of NPrCAP/M-mediated hyperthermia on B16 melanoma subcutaneously transplanted into flanks of mice [23]. In the present study, NPrCAP/M-mediated hyperthermia was performed on subcutaneous melanoma in the hind foot pad to confine the DLN to the inguinal and popliteal lymph nodes [26]. Figure 1A shows the temperature at the tumor surface and in the rectum during AMF

irradiation. The AMF was applied for 30 min. The tumor temperature reached 43°C within 3 min and was maintained at 43°C by controlling the magnetic field intensity. By contrast, the rectal temperature remained at 36°C. These results indicate that a hyperthermia system using NPrCAP/M is able to selectively heat the tumor. In addition, the tumor temperature was maintained precisely within a small standard deviation, thus demonstrating the ease of temperature control by adjusting the magnetic field intensity. FIGURE 1B shows tumor weight on day 17. Tumor growth was significantly suppressed by NPrCAP/M-mediated hyperthermia treatment. In this study, we set the tumor temperature at 43°C and hyperthermia was applied once a day every other day for a total of three treatments, although this was insufficient to achieve complete regression of the B16 melanoma. The NPrCAP/M-mediated hyperthermia system can generate higher temperatures. For example, complete regression of B16 melanoma was observed in 90% of mice at 46°C applied once daily for 2 days [34]. In the present study, we employed relatively moderate conditions for hyperthermia treatment because the heat-generated immunological effect was more significant at 43°C than at 46°C [23]. In agreement with previous results [22,23], substantial amounts of $CD8^+$ T cells were observed around the tumor (FIGURE 1C) and slightly within the tumor (FIGURE 1D) on day 17, while few or no $CD8^+$ T cells were observed around and within the tumor of untreated tumor-bearing mice (without NPrCAP/M injection; data not shown) and NPrCAP/M-injected mice without AMF exposure (data not shown).

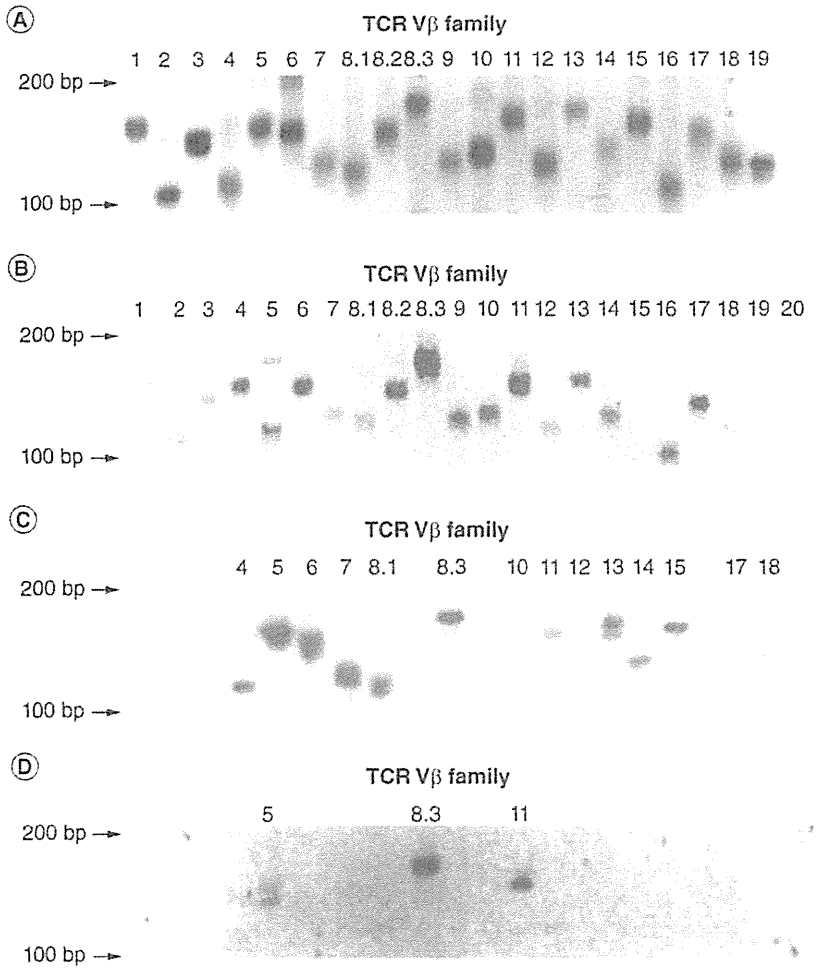

Figure 3. T-cell receptor β-chain gene expression in tumor-infiltrating lymphocytes after *N*-propionyl-4-*S*-cysteaminylphenol/magnetite-mediated hyperthermia. Analysis of each specimen included 22 separate electrophoreses of DNA amplified with different primer sets of each TCR Vβ family gene-specific oligonucleotide. Representative results from Vβ amplifications of T cells in single mice are shown. **(A)** Inguinal lymph node from a naive mouse. **(B)** Inguinal draining lymph node from untreated tumor-bearing mice. **(C)** Inguinal draining lymph node from the mice treated with hyperthermia. **(D)** Tumor from the mice treated with hyperthermia. The TCR Vβ family number is shown above each lane where bands were observed. TCR: T-cell receptor.

Lymph node enlargement after NPrCAP/M-mediated hyperthermia

As shown in FIGURE 2B, enlargement of inguinal DLNs was observed after NPrCAP/M-mediated hyperthermia compared with inguinal non-DLNs on day 17 (FIGURE 2A). As lymph node enlargement is consistently observed in situations of tumor involvement [35], significant enlargement of inguinal DLNs was observed in all tumor-bearing mice, including untreated mice and NPrCAP/M-injected mice (FIGURE 2C). In particular, the inguinal DLNs of tumor-bearing mice treated with NPrCAP/M-mediated hyperthermia were drastically enlarged compared with those of naive mice. The lymph node enlargement may have been due to an increased homing of circulating T cells in response to tumor antigen, and specific T-cell clones may have expanded and differentiated in the DLNs of tumor-bearing mice. We thus compared the number of $CD8^+$ T cells in inguinal lymph nodes of naive mice and inguinal DLNs of tumor-bearing mice treated with NPrCAP/M-mediated hyperthermia. As shown in FIGURE 2D, the number of $CD8^+$ T cells in inguinal DLNs increased significantly in the mice treated with NPrCAP/M-mediated hyperthermia on day 17.

TCR repertoires of TILs after NPrCAP/M-mediated hyperthermia

FIGURE 3 shows representative photographs of the TCR repertoire analysis of an inguinal

lymph node from single mice. In a naive mouse (FIGURE 3A), *TCR* gene expressions of all 21 displayable Vβ families, with the exception of Vβ20, were observed. In DLN from untreated tumor-bearing mice (FIGURE 3B), expressions of 19 *TCR Vβ* genes of 21 Vβ families were observed. In tumor samples from untreated tumor-bearing mice, however, no *TCR* gene expression was observed (data not shown), indicating that few TILs were present in the tumors without hyperthermia treatment. On the other hand, the TCR Vβ repertoire was restricted in the DLNs from the tumor-bearing mouse treated with NPrCAP/M-mediated hyperthermia, and expressions of 14 *TCR Vβ* genes of 21 Vβ families were observed (FIGURE 3C). The TCR repertoire was further restricted in the TILs from tumor samples treated with NPrCAP/M-mediated hyperthermia, and *TCR* gene expression in Vβ-5, -8.3 and -11 was observed in a single mouse (FIGURE 3D), suggesting the clonal expansion of TILs upon antigen recognition. It is believed that the V(D)J junctional sequences are unique to each T-cell clonotype and contribute to TCR diversity. FIGURE 4 shows the sequences of V(D)J junctions of the TCR β chains. For DNA sequencing, the tumor samples from five mice were mixed and analyzed, and we obtained one Vβ6, five Vβ8.2, six Vβ11 and one Vβ15 clone derived from PCR products. Sequence analysis of the PCR clones from TILs revealed a frame shift in the V(D)J region of the *TCR Vβ15* clone (data not shown), suggesting that *TCR Vβ15* would not be functionally generated in this clone. All five *TCR Vβ8.2* clones possessed an identical sequence (FIGURE 4B). On the other hand, sequence analysis revealed that *TCR Vβ11* clones comprised two distinct *Jβ* genes, *Jβ2-3* (three of six clones) and *Jβ2-7* (three of six clones), and three distinct N-Dβ-N regions (FIGURE 4C), indicating oligoclonal expansion of *TCR Vβ11*$^+$ T cells in the tumor.

Restricted usage of *TCR V* genes by T cells that recognize tumor antigens is controversial. In some studies, limited *TCR V* gene usage was found [36,37], while other reports demonstrated diverse *TCR V* usage by TILs [38,39]. In the present study, the TCR Vβ repertoire was limited in TILs from mice that underwent hyperthermia (FIGURE 3), suggesting that TILs were specifically reactive against tumor antigens. However, the use of the TCR Vβ family was not restricted in several experiments, including the results shown in FIGURE 3 (Vβ-5, -8.3 and -11) and FIGURE 4 (Vβ-6, -8.2, -11 and -15). On the other hand, Vβ11 gene expression was primarily found in several experiments (data not shown). In addition to the qualitative analysis of Vβ11 gene expression by reverse-transcription PCR (FIGURES 3 & 4), flow cytometric analysis revealed a quantitative increase in CD8$^+$/TCR Vβ11$^+$ TILs (FIGURE 5A–5C). Harada *et al.* established a B16 melanoma-specific CD8$^+$ T-cell line, AB1, from the spleen cells of mice cured of B16 melanoma with IL-12 treatment [40]. The AB1 cells exclusively expressed *TCR Vβ11*. These results suggest that clonal expansion of Vβ11$^+$ TILs can be a useful marker to investigate the T-cell response to B16 melanoma. The AB1 cells could also recognize TRP-2 peptide as well as B16 melanoma cells. Moreover, Singh *et al.* generated a TRP-2 peptide-specific CD8$^+$ T-cell clone, and spectratype analysis revealed that the cell clone expressed Vβ11 [41]. We thus investigated the reactivity of TILs to melanoma-associated antigens. Lymphocytes from DLNs in tumor-bearing mice treated with hyperthermia using NPrCAP/M were stimulated with the immunodominant peptides of the mouse melanoma-associated antigens TRP-1, TRP-2 or glycoprotein 100, as well as B16F1 cells treated with mitomycin C. These peptide-stimulated lymphocytes were tested

	Vβ6	N-Dβ-N	Jβ1-1	Frequency
Ⓐ	TGTGCCAGCAG	CCCTGGACGG	AACACAGAA	1/1
	C A S S	P G R	N T E	
	Vβ8.2	**N-Dβ-N**	**Jβ2-4**	**Frequency**
Ⓑ	GCCAGCGGTG	CAGACAGT	AGTCAAAAC	5/5
	A S G	A D S	S Q N	
	Vβ11	**N-Dβ-N**	**Jβ2-7**	**Frequency**
Ⓒ	GCAAGCAGCTTAGA	ACTGGGGGGGCGA	GAACAGTAC	3/6
	A S S L E	L G G R	E Q Y	
			Jβ2-3	
	GCAAGCAGC	TCACTGCTT	AGTGCAGAA	1/6
	A S S	S L L	S A E	
			Jβ2-3	
	GCAAGCAGC	TCACTGTTT	AGTGCAGAA	2/6
	A S S	S L F	S A E	

Figure 4. T-cell receptor β junctional sequences from tumor-infiltrating lymphocytes in the mice treated with *N*-propionyl-4-*S*-cysteaminylphenol/magnetite-mediated hyperthermia. (A–C) Nucleotide and predicted amino acid sequences from V(D)J regions of **(A)** *TCR Vβ6*, **(B)** *Vβ8.2* and **(C)** *Vβ11*. Tumor samples from five mice were mixed and analyzed. The amplified PCR products of the *TCR Vβ* gene were cloned into the plasmid vector. Six or as many as possible randomly picked colonies were analyzed, and the plasmid DNA from the positive colonies was sequenced.
D: Diversity; J: Joining; V: Variable.

doi:10.2217/NNM.12.142

for the ability to recognize the antigens by releasing IFN-γ as an assay to detect T cells with high avidity toward the tumor antigen. As shown in FIGURE 5D, only the lymphocytes stimulated with TRP-2 peptide displayed a significant IFN-γ release, suggesting restricted reactivity toward the TRP-2 antigen. A further important point is whether TRP-2 peptide can be used to boost anti-tumor immunity induced by NPrCAP/M-mediated hyperthermia. One direction for future research might be the development of a combination therapy of NPrCAP/M-mediated hyperthermia with a TRP-2 peptide vaccine.

To the best of our knowledge, this is the first report to determine the V(D)J junctional sequence of the *TCR Vβ11* gene of TILs in B16 melanoma. This information is very useful, not only to understand the T-cell response to B16 melanoma, but also to develop more effective cancer immunotherapy. Immunotherapy with adoptive cell transfer using TILs has proven to be a useful strategy for the treatment of metastatic melanoma [42]. Recent strategies involve cloning of *TCR αβ* genes specific for melanoma-associated antigens from TILs and retrovirally transducing these genes into peripheral blood lymphocytes [43]. Information on Vβ11 usage

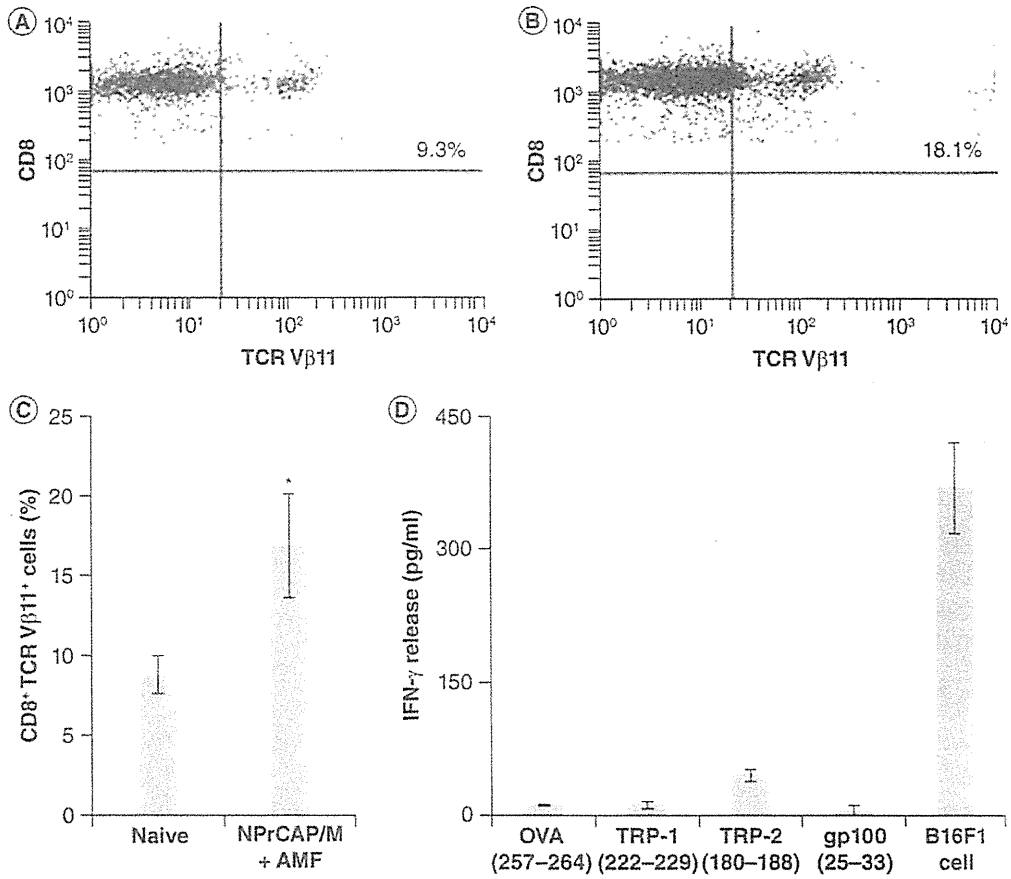

Figure 5. T-cell response in the mice treated with *N*-propionyl-4-*S*-cysteaminylphenol/magnetite-mediated hyperthermia. (A–C) Flow cytometric analysis of CD8+/TCR Vβ11+ T cells in **(A)** an inguinal lymph node of a naive mouse and **(B)** an inguinal draining lymph node of a mouse treated with NPrCAP/M-mediated hyperthermia. CD8+ T cells in the lymph node were purified by magnetic cell sorting, and the representative data from **(A & B)** single mice and **(C)** five mice for statistical analysis are shown. Data are the means and standard deviations. **(D)** T-cell response to melanoma-associated antigen peptides. After the hyperthermia treatment, draining lymph nodes from five mice were harvested on day 17, and lymphocytes were then restimulated *in vitro* with antigen peptides or mitomycin-treated B16F1 cells for 5 days. $OVA_{257-264}$ peptide was used as a negative control. After the restimulation, culture supernatants were collected and amounts of IFN-γ were measured by ELISA. Data are the means and standard deviations of triplicate experiments. *$p < 0.01$.
AMF: Alternating magnetic field; gp: Glycoprotein; NPrCAP/M: *N*-propionyl-4-*S*-cysteaminylphenol/magnetite; OVA: Ovalbumin; TCR: T-cell receptor; TRP: Tyrosinase-related protein.

in TILs and the V(D)J junctional sequence will be useful to further determine the Vα gene for reconstitution of functional T cells by *TCR αβ* gene transfer. We are now determining the *Vα* gene to reconstitute functional T cells to investigate whether Vβ11$^+$ TILs are CTLs that actually play a crucial role in *in vivo* immune responses against B16 melanoma, and whether adoptive immunotherapy using *TCR* gene-engineered CTLs is possible to enhance the therapeutic effects of NPrCAP/M-mediated hyperthermia.

Conclusion

In this study, we analyzed the diversity of TCRs in TILs after NPrCAP/M-mediated hyperthermia. It was found that T cells were clonally expanded in B16 tumors after hyperthermia, in which Vβ11$^+$ T cells were preferentially expanded. The DNA sequences of the CDR3 of the TCR β-chain in TILs revealed the presence of clonally expanded T cells. These results indicate that the T-cell response in B16 melanoma after hyperthermia is dominated by T cells directed toward a limited number of epitopes and that epitope-specific T cells frequently use a restricted TCR repertoire.

Future perspective

Although early lesions of primary melanoma are curable by excision, successful treatment of metastatic melanoma has been elusive. Recently, the authors have proceeded to a Phase I/II study of the effect of NPrCAP/M-mediated hyperthermia not only on treated primary tumors but also on nontreated metastatic tumors [44]. The therapeutic protocol followed the animal experiments. However, NPrCAP/M was made by conjugating polyethylene glycol between NPrCAP and magnetite nanoparticles, and a new AMF applicator called a 'ferrite core-inserted solenoid type' [11] was utilized in the clinical trials. The future potential use of this technology is illustrated in Figure 6.

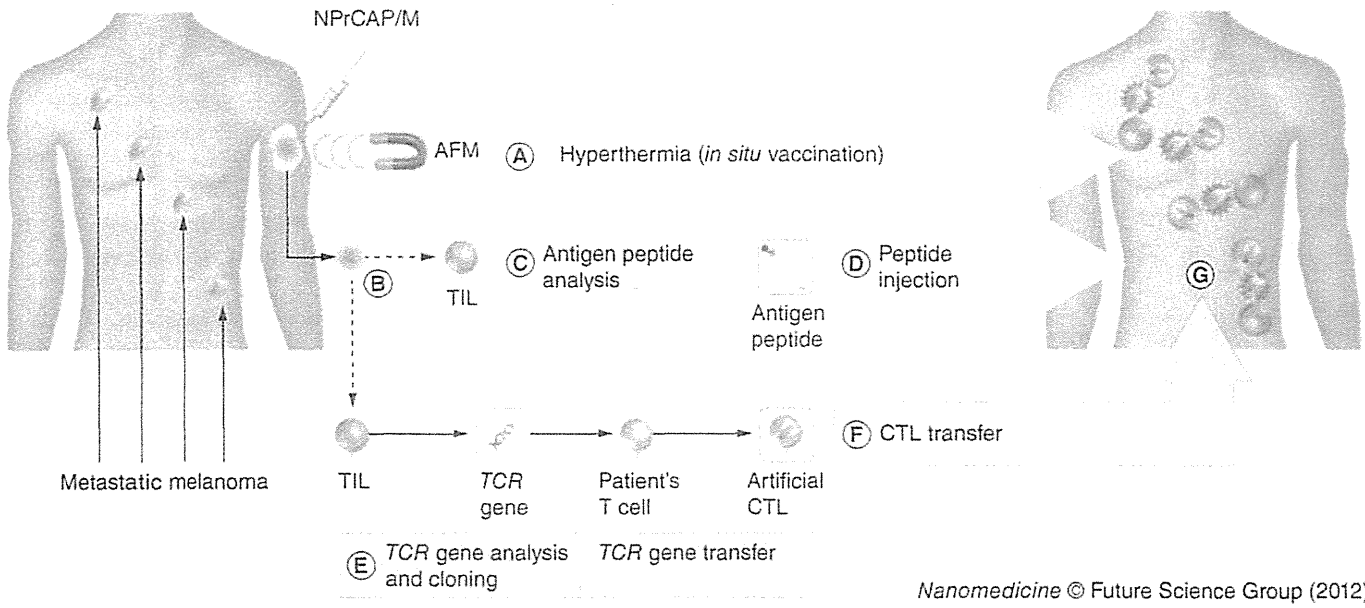

Figure 6. Future potential of *N*-propionyl-4-*S*-cysteaminylphenol/magnetite-mediated hyperthermia for melanoma-targeted thermo-immunotherapy. This strategy is based on combinations of hyperthermia using NPrCAP/M with antimelanoma peptide vaccine and *TCR* gene-engineered CTL therapy. **(A)** NPrCAP/M-mediated hyperthermia system confers anti-tumor immunity via release of heat-shock protein–peptide complexes during necrotic tumor cell death *in vivo*, which we have termed '*in situ* vaccination'. **(B)** The primary melanoma is exploited to provide tumor antigens to the immune system for 2 weeks, and then the melanoma is excised surgically to analyze TILs. **(C)** Melanoma-specific antigen peptides are analyzed by using TILs. **(D)** The screened peptides can be used to boost anti-tumor immunity induced by hyperthermia. For mouse B16 melanoma, TRP-2 peptide will be used to boost anti-tumor immunity induced by NPrCAP/M-mediated hyperthermia. **(E)** *TCR* genes of TILs are analyzed and cloned. **(F)** Adoptive immunotherapy using *TCR* gene-engineered CTL therapy will enhance the therapeutic effects of NPrCAP/M-mediated hyperthermia. For B16 melanoma, DNA sequences of TCRb CDR3 of TILs (see Figure 4) can be used. **(G)** Taken together, the combination of antimelanoma peptide vaccine and TCR gene-engineered CTL therapy with NPrCAP/M-mediated hyperthermia is a promising treatment for improving clinical effects, especially for patients with early metastatic melanomas because of the induction of systemic antimelanoma immunity.
AMF: Alternating magnetic field; CTL: Cytotoxic T lymphocyte; NPrCAP/M: *N*-propionyl-4-*S*-cysteaminylphenol/magnetite; TCR: T-cell receptor; TIL: Tumor-infiltrating lymphocyte.

doi:10.2217/NNM.12.142

Financial & competing interests disclosure

This work was supported by Health and Labour Sciences Research Grants-in-Aid (H21-nano-006) for Research on Advanced Medical Technology from the Ministry of Health, Labour and Welfare of Japan. The authors have no other relevant affiliations or financial involvement with any organization or entity with a financial interest in or financial conflict with the subject matter or materials discussed in the manuscript apart from those disclosed.

No writing assistance was utilized in the production of this manuscript.

Ethical conduct of research

The authors state that they have obtained appropriate institutional review board approval or have followed the principles outlined in the Declaration of Helsinki for all human or animal experimental investigations. In addition, for investigations involving human subjects, informed consent has been obtained from the participants involved.

Executive summary

Hyperthermia using N-propionyl-4-S-cysteaminylphenol/magnetite for melanoma

- Hyperthermia using *N*-propionyl-4-*S*-cysteaminylphenol/magnetite (NPrCAP/M) was able to selectively heat transplanted melanomas by direct injection of NPrCAP/M.
- Tumor growth was significantly suppressed by the treatment of NPrCAP/M-mediated hyperthermia.

Anti-tumor immunity induced by NPrCAP/M-mediated hyperthermia

- $CD8^+$ T cells were infiltrated within the tumor after hyperthermia.
- Lymph node enlargement was observed after hyperthermia.

T-cell receptor repertoire analysis of tumor-infiltrating lymphocytes after NPrCAP/M-mediated hyperthermia

- Restricted T-cell receptor repertoire was observed in the tumor-infiltrating lymphocytes (TILs).
- Expansion of $V\beta11^+$ T cells was primarily found in the TILs.
- DNA sequences of T-cell receptor β CDR3 of TILs were identified.

References

Papers of special note have been highlighted as:
- of interest
- of considerable interest

1 Dewhirst MW, Prosnitz L, Thrall D *et al.* Hyperthermic treatment of malignant diseases: current status and a view toward the future. *Semin. Oncol.* 24(6), 616–625 (1997).

2 van der Zee J. Heating the patient: a promising approach? *Ann. Oncol.* 13(8), 1173–1184 (2002).

3 Shecterle LM, St Cyr JA. Whole body hyperthermia as a potential therapeutic option. *Cancer Biother.* 10(4), 253–256 (1995).

4 Storm FK, Morton DL, Kaiser LR *et al.* Clinical radiofrequency hyperthermia: a review. *Natl Cancer Inst. Monogr.* 61, 343–350 (1982).

5 Gazeau F, Lévy M, Wilhelm C. Optimizing magnetic nanoparticle design for nanothermotherapy. *Nanomedicine (Lond.)* 3(6), 831–844 (2008).

- **Comprehensive review of hyperthermia using magnetite nanoparticles, including anti-tumor immune response induced by hyperthermia.**

6 Jordan A, Scholz R, Wust P *et al.* Effects of magnetic fluid hyperthermia (MFH) on C3H mammary carcinoma *in vivo*. *Int. J. Hyperthermia* 13(6), 587–605 (1997).

7 Ito A, Shinkai M, Honda H *et al.* Medical application of functionalized magnetic nanoparticles. *J. Biosci. Bioeng.* 100(1), 1–11 (2005).

8 Jordan A, Wust P, Fähling H *et al.* Inductive heating of ferrimagnetic particles and magnetic fluids: physical evaluation of their potential for hyperthermia. *Int. J. Hyperthermia.* 9(1), 51–68 (1993).

- **First paper describing physical mechanisms of hyperthermia using magnetite nanoparticles.**

9 Ito A, Kuga Y, Honda H *et al.* Magnetite nanoparticle-loaded anti-HER2 immunoliposomes for combination of antibody therapy with hyperthermia. *Cancer Lett.* 212(2), 167–175 (2004).

10 Cole AJ, Yang VC, David AE. Cancer theranostics: the rise of targeted magnetic nanoparticles. *Trends Biotechnol.* 29(7), 323–332 (2011).

11 Kawai N, Ito A, Nakahara Y *et al.* Complete regression of experimental prostate cancer in nude mice by repeated hyperthermia using magnetite cationic liposomes and a newly developed solenoid containing a ferrite core. *Prostate* 66(7), 718–727 (2006).

12 Gneveckow U, Jordan A, Scholz R *et al.* Description and characterization of the novel hyperthermia- and thermoablation-system MFH 300F for clinical magnetic fluid hyperthermia. *Med. Phys.* 31(6), 1444–14451 (2004).

13 Thiesen B, Jordan A. Clinical applications of magnetic nanoparticles for hyperthermia. *Int. J. Hyperthermia.* 24(6), 467–474 (2008).

14 Shinkai M, Le B, Honda H *et al.* Targeting hyperthermia for renal cell carcinoma using human MN antigen-specific magnetoliposomes. *Jpn. J. Cancer Res.* 92(10), 1138–1145 (2001).

15 Gupta AK, Naregalkar RR, Vaidya VD *et al.* Recent advances on surface engineering of magnetic iron oxide nanoparticles and their biomedical applications *Nanomedicine (Lond.)* 2(1), 23–39 (2007).

- **Review of procedures for synthesis and surface coating of magnetite nanoparticles.**

16 Yiu HH. Engineering the multifunctional surface on magnetic nanoparticles for targeted biomedical applications: a chemical approach. *Nanomedicine (Lond.)* 6(8), 1429–1446 (2011).

17 Thomas PD, Kishi H, Cao H *et al.* Selective incorporation and specific cytocidal effect as the cellular basis for the antimelanoma action of sulphur containing tyrosine analogs. *J. Invest. Dermatol.* 113(6), 928–934 (1999).

18 Sato M, Yamashita T, Ohkura M *et al.* *N*-propionyl-cysteaminylphenol-magnetite conjugate (NPrCAP/M) is a nanoparticle for the targeted growth suppression of melanoma cells. *J. Invest. Dermatol.* 129(9), 2233–2241 (2009).

19 Johannsen M, Gneveckow U, Eckelt L *et al.* Clinical hyperthermia of prostate cancer using magnetic nanoparticles: presentation of a new interstitial technique. *Int. J. Hyperthermia* 21(7), 637–647 (2005).

20 Ito A, Shinkai M, Honda H *et al.* Heat shock protein 70 expression induces antitumor immunity during intracellular hyperthermia using magnetite nanoparticles. *Cancer Immunol. Immunother.* 52(2), 80–88 (2003).

21 Ito A, Honda H, Kobayashi T. Cancer immunotherapy based on intracellular hyperthermia using magnetite nanoparticles: a novel concept of 'heat-controlled necrosis' with heat shock protein expression. *Cancer Immunol. Immunother.* 55(3), 320–328 (2006).

22 Sato A, Tamura Y, Sato N *et al.* Melanoma-targeted chemo-thermo-immuno (CTI)-therapy using *N*-propionyl-4-*S*-cysteaminylphenol-magnetite nanoparticles elicits CTL response via heat shock protein–peptide complex release. *Cancer Sci.* 101(9), 1939–1946 (2010).

23 Takada T, Yamashita T, Sato M *et al.* Growth inhibition of re-challenge B16 melanoma transplant by conjugates of melanogenesis substrate and magnetite nanoparticles as the basis for developing melanoma-targeted chemo-thermo-immunotherapy. *J. Biomed. Biotechnol.* 457936 (2009).

24 Galon J, Costes A, Sanchez-Cabo F *et al.* Type, density, and location of immune cells within human colorectal tumors predict clinical outcome. *Science* 313(5795), 1960–1964 (2006).

25 Davis MM, Bjorkman PJ. T-cell antigen receptor genes and T-cell recognition. *Nature* 334(6181), 395–402 (1988).

26 Harrell MI, Iritani BM, Ruddell A. Lymph node mapping in the mouse. *J. Immunol. Methods* 332(1–2), 170–174 (2008).

27 Hindley JP, Ferreira C, Jones E *et al.* Analysis of the T-cell receptor repertoires of tumor-infiltrating conventional and regulatory T cells reveals no evidence for conversion in carcinogen-induced tumors. *Cancer Res.* 71(3), 736–746 (2011).

28 Godebu E, Summers-Torres D, Lin MM *et al.* Polyclonal adaptive regulatory CD4 cells that can reverse Type I diabetes become oligoclonal long-term protective memory cells. *J. Immunol.* 181(3), 1798–1805 (2008).

29 Böhm W, Thoma S, Leithäuser F *et al.* T cell-mediated, IFN-gamma-facilitated rejection of murine B16 melanomas. *J. Immunol.* 161(2), 897–908 (1998).

30 Dyall R, Bowne WB, Weber LW *et al.* Heteroclitic immunization induces tumor immunity. *J. Exp. Med.* 188(9), 1553–1561 (1998).

31 Bloom MB, Perry-Lalley D, Robbins PF *et al.* Identification of tyrosinase-related protein 2 as a tumor rejection antigen for the B16 melanoma. *J. Exp. Med.* 185(3), 453–459 (1997).

32 Zhai Y, Yang JC, Spiess P *et al.* Cloning and characterization of the genes encoding the murine homologues of the human melanoma antigens MART1 and gp100. *J. Immunother.* 20(1), 15–25 (1997).

33 Rötzschke O, Falk K, Stevanović S *et al.* Exact prediction of a natural T cell epitope. *Eur. J. Immunol.* 21(11), 2891–2894 (1991).

34 Suzuki M, Shinkai M, Honda H *et al.* Anticancer effect and immune induction by hyperthermia of malignant melanoma using magnetite cationic liposomes. *Melanoma Res.* 13(2), 129–135 (2003).

35 Salameire D, Le Bris Y, Fabre B *et al.* Efficient characterization of the TCR repertoire in lymph nodes by flow cytometry. *Cytometry A* 75(9), 743–751 (2009).

- **Large-scale analysis of the T-cell receptor (TCR) repertoire in lymph nodes using flow cytometry.**

36 Nitta T, Oksenberg JR, Rao NA *et al.* Predominant expression of T cell receptor V alpha 7 in tumor-infiltrating lymphocytes of uveal melanoma. *Science* 249(4969), 672–674 (1990).

- **Analysis of *TCR Vα* gene expression in tumor-infiltrating lymphocytes within human melanoma.**

37 Solheim JC, Alexander-Miller MA, Martinko JM *et al.* Biased T cell receptor usage by Ld-restricted, tum-peptide-specific cytotoxic T lymphocyte clones. *J. Immunol.* 150(3), 800–811 (1993).

38 Ferradini L, Roman-Roman S, Azocar J *et al.* Analysis of T-cell receptor alpha/beta variability in lymphocytes infiltrating a melanoma metastasis. *Cancer Res.* 52(17), 4649–4654 (1992).

39 Shilyansky J, Nishimura MI, Yannelli JR *et al.* T-cell receptor usage by melanoma-specific clonal and highly oligoclonal tumor-infiltrating lymphocyte lines. *Proc. Natl Acad. Sci. USA* 91(7), 2829–2833 (1994).

- **Analysis of the diversity of TCRs involved in human melanoma antigen recognition.**

40 Harada M, Tamada K, Abe K *et al.* Characterization of B16 melanoma-specific cytotoxic T lymphocytes. *Cancer Immunol. Immunother.* 47(4), 198–204 (1998).

- **Establishment of B16 melanoma-specific CTL clone characterized by TCR Vβ11 expression and TRP-2 peptide antigen-specific cytotoxicity.**

41 Singh V, Ji Q, Feigenbaum L *et al.* Melanoma progression despite infiltration by *in vivo*-primed TRP-2-specific T cells. *J. Immunother.* 32(2), 129–139 (2009).

42 Rosenberg SA, Restifo NP, Yang JC *et al.* Adoptive cell transfer: a clinical path to effective cancer immunotherapy. *Nat. Rev. Cancer* 8(4), 299–308 (2008).

43 Park TS, Rosenberg SA, Morgan RA. Treating cancer with genetically engineered T cells. *Trends Biotechnol.* 29(11), 550–557 (2011).

- **Review of *TCR* gene-engineered T cells.**

44 Jimbow K, Tamura Y, Yoneta A *et al.* Conjugation of magnetite nanoparticles with melanogenesis substrate, NPrCAP provides melanoma targeted, *in situ* peptide vaccine immunotherapy through HSP production by chemo-thermotherapy. *J. Biomater. Nanobiotechnol.* 3(2), 140–153 (2012).

Affiliations

- **Akira Ito**
  Department of Chemical Engineering, Faculty of Engineering, Kyushu University, 744 Motooka, Nishi-ku, Fukuoka 819-0395, Japan
- **Masaki Yamaguchi**
  Department of Chemical Engineering, Faculty of Engineering, Kyushu University, 744 Motooka, Nishi-ku, Fukuoka 819-0395, Japan
- **Noriaki Okamoto**
  Department of Chemical Engineering, Faculty of Engineering, Kyushu University, 744 Motooka, Nishi-ku, Fukuoka 819-0395, Japan
- **Yuji Sanematsu**
  Department of Chemical Engineering, Faculty of Engineering, Kyushu University, 744 Motooka, Nishi-ku, Fukuoka 819-0395, Japan
- **Yoshinori Kawabe**
  Department of Chemical Engineering, Faculty of Engineering, Kyushu University, 744 Motooka, Nishi-ku, Fukuoka 819-0395, Japan
- **Kazumasa Wakamatsu**
  Department of Chemistry, Fujita Health University School of Health Sciences, Toyoake 470-1192, Japan
- **Shosuke Ito**
  Department of Chemistry, Fujita Health University School of Health Sciences, Toyoake 470-1192, Japan
- **Hiroyuki Honda**
  Department of Biotechnology, School of Engineering, Nagoya University, Nagoya 464-8603, Japan
- **Takeshi Kobayashi**
  School of Bioscience and Biotechnology, Chubu University, Kasugai 487-8501, Japan
- **Eiichi Nakayama**
  Faculty of Health and Welfare, Kawasaki University of Medical Welfare, Kurasiki 701-0193, Japan

doi:10.2217/NNM.12.142

- Yasuaki Tamura
  First Department of Pathology, Sapporo Medical University School of Medicine, Sapporo 060-8556, Japan
- Masae Okura
  Department of Dermatology, Sapporo Medical University School of Medicine, Sapporo 060-8543, Japan
- Toshiharu Yamashita
  Department of Dermatology, Sapporo Medical University School of Medicine, Sapporo 060-8543, Japan
- Kowichi Jimbow
  Department of Dermatology, Sapporo Medical University School of Medicine, Sapporo 060-8543, Japan
- Masamichi Kamihira
  Department of Chemical Engineering, Faculty of Engineering, Kyushu University, 744 Motooka, Nishi-ku, Fukuoka 819-0395, Japan

Vaccine 31 (2013) 2110–2118

Contents lists available at SciVerse ScienceDirect

Vaccine

journal homepage: www.elsevier.com/locate/vaccine

Establishment of animal models to analyze the kinetics and distribution of human tumor antigen-specific CD8$^+$ T cells

Daisuke Muraoka[a,d], Hiroyoshi Nishikawa[a,e,*], Takuro Noguchi[a,f], Linan Wang[b], Naozumi Harada[a,d], Eiichi Sato[g], Immanuel Luescher[h], Eiichi Nakayama[i], Takuma Kato[c], Hiroshi Shiku[a,b,1]

[a] Departments of Cancer Vaccine, Mie University Graduate School of Medicine, Mie 514-8507, Japan
[b] Departments of Immuno-Gene Therapy, Mie University Graduate School of Medicine, Mie 514-8507, Japan
[c] Departments of Cellular and Molecular Immunology, Mie University Graduate School of Medicine, Mie 514-8507, Japan
[d] Immunofrontier, Inc., Tokyo, 143-0023, Japan
[e] Experimental Immunology, Immunology Frontier Research Center, Osaka University, Osaka, 565-0871, Japan
[f] Ludwig Institute for Cancer Research, New York Branch, Memorial Sloan-Kettering Cancer Center, New York, NY 10065, United States
[g] Department of Anatomic Pathology, Tokyo Medical University, Tokyo, 160-8402, Japan
[h] Ludwig Institute for Cancer Research, Lausanne Branch, University of Lausanne, Epalinges, 1066, Switzerland
[i] Faculty of Health and Welfare, Kawasaki University of Medical Welfare, Okayama, 701-0193, Japan

ARTICLE INFO

Article history:
Received 21 January 2013
Accepted 27 February 2013
Available online 13 March 2013

Keywords:
Translational research
Animal model
Cancer vaccine
Immune responses
CD8$^+$ T cells
Cacer/testis antigens

ABSTRACT

Many patients develop tumor antigen-specific T cell responses detectable in peripheral blood mononuclear cells (PBMCs) following cancer vaccine. However, measurable tumor regression is observed in a limited number of patients receiving cancer vaccines. There is a need to re-evaluate systemically the immune responses induced by cancer vaccines. Here, we established animal models targeting two human cancer/testis antigens, NY-ESO-1 and MAGE-A4. Cytotoxic T lymphocyte (CTL) epitopes of these antigens were investigated by immunizing BALB/c mice with plasmids encoding the entire sequences of NY-ESO-1 or MAGE-A4. CD8$^+$ T cells specific for NY-ESO-1 or MAGE-A4 were able to be detected by ELISPOT assays using antigen presenting cells pulsed with overlapping peptides covering the whole protein, indicating the high immunogenicity of these antigens in mice. Truncation of these peptides revealed that NY-ESO-1-specific CD8$^+$ T cells recognized D^d-restricted 8mer peptides, NY-ESO-1$_{81-88}$. MAGE-A4-specific CD8$^+$ T cells recognized D^d-restricted 9mer peptides, MAGE-A4$_{265-273}$. MHC/peptide tetramers allowed us to analyze the kinetics and distribution of the antigen-specific immune responses, and we found that stronger antigen-specific CD8$^+$ T cell responses were required for more effective anti-tumor activity. Taken together, these animal models are valuable for evaluation of immune responses and optimization of the efficacy of cancer vaccines.

1. Introduction

A number of cancer vaccine strategies targeting tumor antigens recognized by the human immune system have been tested [1–3]. While many of these cancer vaccines elicited measurable immune responses detectable in peripheral blood mononuclear cells (PBMCs), only a subset of treated patients experienced clinical benefits, such as tumor regression [4,5]. Because of the weak clinical effectiveness of currently available cancer vaccines, not only new immunogenic antigens, effective adjuvant formulations, vectors or vaccination methods but also new methodologies to evaluate efficacy of cancer vaccines are required.

NY-ESO-1, a germ line cell protein detected by SEREX (serological identification of antigens by recombinant expression cloning) using the serum of an esophageal cancer patient, is often expressed by cancer cells, but not by normal somatic cells [3,6]. This ideal expression pattern facilitated the study of this antigen; including immuno-monitoring of cancer patients with NY-ESO-1-expressing tumors and clinical trials that focused on NY-ESO-1 [3]. While these studies have revealed that a number of different cancer vaccines, including short and overlapping peptides, protein, viral vectors and DNA, resulted in development of measurable immune responses,

Abbreviations: APC, antigen presenting cells; CTL, cytotoxic T lymphocyte; dLN, draining lymph node; ELISPOT assay, enzyme-linked immunospot assay; IFN, interferon; mAb, monoclonal antibody; PBMC, peripheral blood mononuclear cells.

* Corresponding author at: Experimental Immunology, Immunology Frontier Research Center, Osaka University, 3-1 Yamadaoka, Suita, Osaka 565-0871, Japan. Tel.: +81 6 6879 4963; fax: +81 6 6879 4464.
E-mail addresses: nisihiro@ifrec.osaka-u.ac.jp (H. Nishikawa), shiku@clin.medic.mie-u.ac.jp (H. Shiku).
[1] Departments of Cancer Vaccine and Immuno-Gene Therapy, Mie University Graduate School of Medicine, 2-174 Edobashi, Tsu, Mie 514-8507, Japan. Tel.: +81 59 231 5062; fax: +81 59 231 5276.

0264-410X/$ – see front matter © 2013 Elsevier Ltd. All rights reserved.
http://dx.doi.org/10.1016/j.vaccine.2013.02.056

correlations between immunological and clinical responses were often week or difficult to observe [3].

MAGE-A4, another cancer/testis (CT) antigen, elicits MAGE-A4-specific $CD4^+$ and $CD8^+$ T cell responses in some patients with MAGE-A4-expressing cancers, indicating that MAGE-A4 is also an immunogenic protein [7–9]. We have recently reported a novel MAGE-A4 epitope presented by human leukocyte antigen (HLA)-A*2402 using a $CD8^+$ T cell clone 2-28 [9]. As this clone effectively killed tumor cell lines that expressed both MAGE-A4 and HLA-A*2402, this antigen could be a candidate for a cancer vaccine.

Given the poor correlation between the immune responses detected in PBMCs and clinical responses [2,3,5], it is necessary to re-evaluate existing cancer immunotherapy strategies in detail using animal models, namely reverse translational research. To this end, we developed animal models involving human tumor antigens, such as NY-ESO-1 or MAGE-A4 in this study.

2. Materials and methods

2.1. Mice

Female BALB/c mice were purchased from SLC Japan (Shizuoka, Japan) and used at 7–10 weeks of age. They were maintained at the Animal Center of Mie University Graduate School of Medicine (Mie, Japan). The experimental protocol was approved by the Ethics Review Committee for Animal Experimentation of Mie University Graduate School of Medicine.

2.2. Antibodies and reagents

Anti-H2-K^d (KD40, mouse IgG2a), anti-H2-D^d (DD98, mouse IgG2a), and anti-H2-L^d (30-5-7, mouse IgG2a) were produced and purified from each hybridoma. FITC-conjugated anti-CD8 mAb (53-6.7, rat IgG2a) and APC-conjugated anti-CD4 mAb (GK1.5, rat IgG2b) were purchased from BD Biosciences (Franklin Lakes, NJ). PE-conjugated anti-Foxp3 mAb (Fjk16s, rat IgG2a) was purchased from eBiosciences (San Diego, CA). Synthetic NY-ESO-1 and MAGE-A4 peptides (summarized in Supplementary Table 1) were obtained from Sigma Genosys (Hokkaido, Japan).

2.3. Immunization using a gene gun

Naive BALB/c mice were immunized twice at two-week intervals. Gold particles coated with 1 μg of each plasmid DNA were prepared and delivered into the shaved skin of the abdominal wall of BALB/c mice using a Helios Gene Gun System (BioRad, Hercules, CA) at a helium discharge pressure of 350–400 psi, as described previously [10,11].

2.4. Cell isolation

Spleen cell suspensions were mixed with CD8 Microbeads (Miltenyi Biotec, Bergisch Gladbach, Germany) and separated into $CD8^+$ T cells by positive selection on a MACS column. The isolated $CD8^+$ T cell populations were confirmed to contain >95% $CD8^+$ T cells.

2.5. Enzyme-linked immunospot (ELISPOT) assay

The number of IFN-γ secreting antigen-specific $CD8^+$ T cells was assessed by ELISPOT assay as described previously [10,11]. Briefly, purified $CD8^+$ T cells were cultured for 24 hours with 5×10^5 irradiated CD90-depleted splenocytes pulsed with the indicated peptides in 96-well nitrocellulose-coated microtiter plates (Millipore, Bedford, MA) coated with rat anti-mouse IFN-γ mAb (R4-6A2, BD Biosciences). Spots were developed using biotinylated anti-mouse IFN-γmAb (XMG1.2, BD Biosciences), alkaline phosphatase conjugated streptavidin (MABTECH, Sweden) and alkaline phosphatase substrate kit (BioRad), and subsequently counted.

2.6. ELISA

96-well flat-bottomed microliter plates (Immuno-NUNC) were coated with 20 ng/50 μml of NY-ESO-1 or MAGE-A4 protein, respectively, at 4 °C overnight. Wells were blocked with 1% BSA/PBS for 1 hour at room temperature and washed three times. Serum (1:100 dilution) was added and incubated at 4 °C overnight. After washing, goat anti-mouse IgG antibody conjugated with horseradish peroxidase (Promega, Madison, WI) was added (1:5000 dilution). Two hours later, color was developed with TMB substrate solution (Thermo scientific, IL) and stopped with H_2SO_4. The absorbance was measured at 450 nm and calculated after subtraction of the absorbance value of control wells without sera.

2.7. Flow cytometry and tetramer staining

Tetramer staining was performed as described previously [11]. Briefly, cells were stained with PE-labeled NY-ESO-$1_{81-88}/D^d$ or MAGE-$A4_{265-273}/D^d$ tetramers (prepared at the Ludwig Institute Core Facility, Lausanne, Switzerland) for 10 minutes at 37 °C before additional staining of surface markers for 15 minutes at 4 °C. After washing, the results were analyzed on FACSCanto (BD Biosciences) and FlowJo software (Tree Star, Ashland, OR).

2.8. Tumors

CT26 is a colon epithelial tumor derived by intrarectal injections of N-nitroso-N-methylurethane in BALB/c mice [12]. CT26 expressing NY-ESO-1 or MAGE-A4, a human cancer/testis antigen were established as described previously [11,13].

2.9. Statistical analysis

Values were expressed as mean ± SD. Differences between groups were examined for statistical significance using the Student's *t*-test. *p* values <0.05 were considered statistically significant.

3. Results

3.1. NY-ESO-1-specific $CD8^+$ T cells recognize D^d-restricted NY-ESO-1_{81-88} peptide

We analyzed the minimal epitope recognized by NY-ESO-1-specific $CD8^+$ T cells after immunization with NY-ESO-1. To this end, we employed a Helios Gene Gun System as we have previously detected NY-ESO-1-specific $CD8^+$ T cell responses [10,11]. To identify minimal epitopes, naive BALB/c mice were immunized twice at two-week intervals with plasmids encoding the entire sequence of NY-ESO-1. $CD8^+$ T cells were obtained from spleens and specific T cell responses were analyzed by ELISPOT assay using peptide pools shown in Supplementary Table 1. A significant number of NY-ESO-1-specific $CD8^+$ T cells was detected against peptide pool #3 (Fig. 1A). To identify the NY-ESO-1 epitope, NY-ESO-1-specific $CD8^+$ T cells were stimulated with each of these peptides. IFN-γ secretion was observed when NY-ESO-1-specific $CD8^+$ T cells were stimulated with 71–90 and 81–100 NY-ESO-1 peptides, suggesting the presence of a minimal epitope within 81–90 residues (Fig. 1B). To determine the minimal epitope, the 81–90 peptide of NY-ESO-1 was further truncated. NY-ESO-1-specific $CD8^+$ T cells recognized the 80–88 and 81–88, but not 80–87 or 82–88 peptides, thus

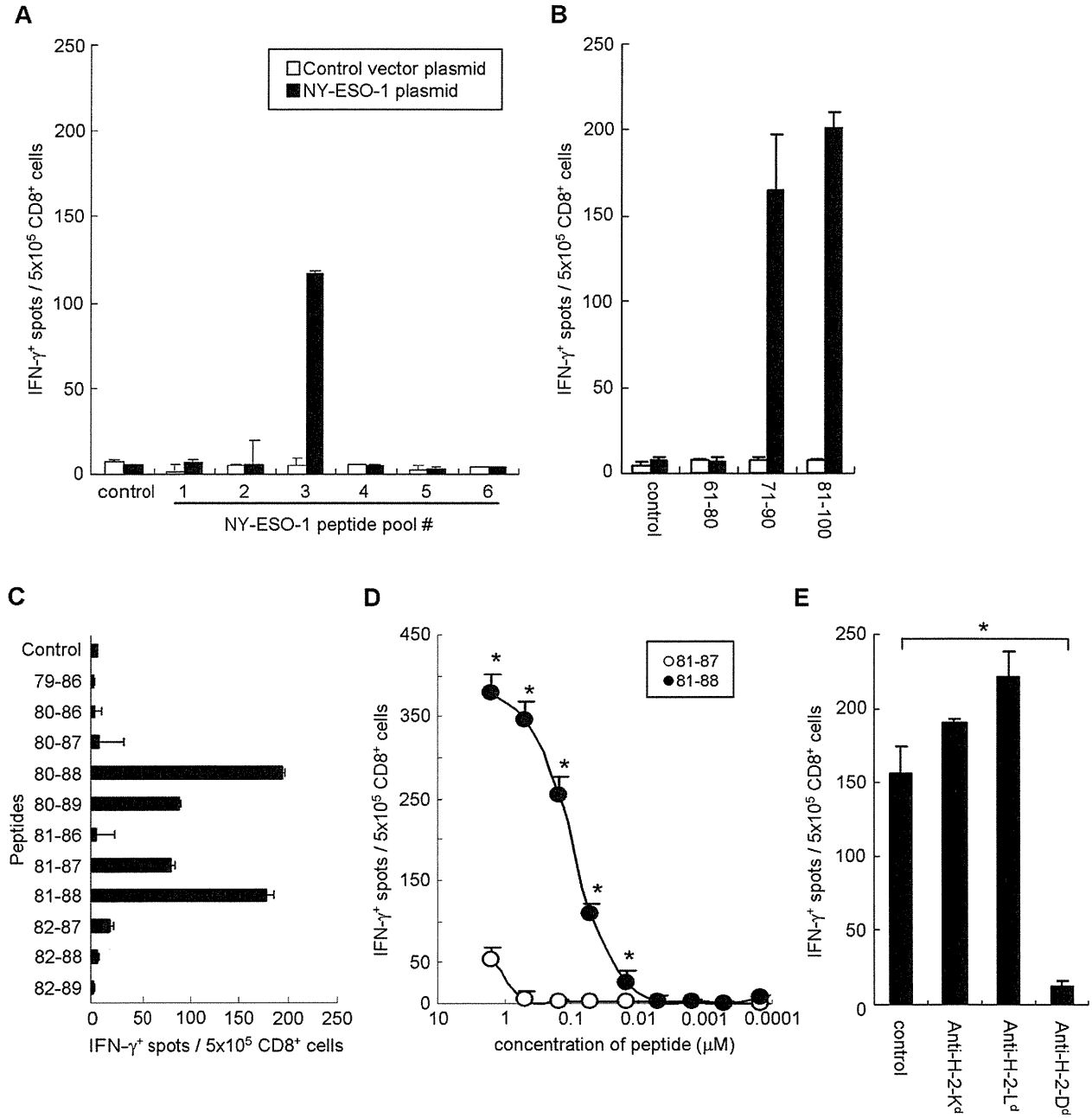

Fig. 1. NY-ESO-1-specific CD8$^+$ T cells recognize D^d-restricted NY-ESO-1$_{81-88}$ peptide. (A–C) BALB/c mice were immunized by gene gun twice at two-week intervals with plasmids encoding the entire sequence of NY-ESO-1. CD8$^+$ T cells were obtained from spleens and specific T cells were analyzed with ELISPOT assay using APCs pulsed with the indicated peptides. (D) Avidity of induced NY-ESO-1-specific CD8$^+$ T cells was analyzed with ELISPOT assay using APCs pulsed with graded doses of peptides ranging from 3 to 0.0001 μM. (E) MHC restriction of induced NY-ESO-1-specific CD8$^+$ T cells was analyzed with ELISPOT assay by the addition of anti-H-2-K^d, anti-H-2-D^d or anti-H-2-L^d mAbs. These experiments were repeated two to four times with similar results. Data are mean ± SD.

the minimal epitope was identified to be NY-ESO-1$_{81-88}$ peptide (Fig. 1C).

To confirm this, graded doses of the peptides were pulsed on antigen presenting cells (APCs) and specific IFN-γ secretion was analyzed by ELISPOT assay. NY-ESO-1-specific CD8$^+$ T cells were high-avidity, and capable to recognize as little as 30 nM of peptide (Fig. 1D), confirming that NY-ESO-1$_{81-88}$ peptide is the minimal epitope. Next, we assessed the restriction of this response using blocking antibodies. NY-ESO-1-specific CD8$^+$ T cell responses were completely blocked by addition of anti-H-2-D^d mAb (Fig. 1E). Taken together, NY-ESO-1-specific CD8$^+$ T cells recognize D^d-restricted NY-ESO-1$_{81-88}$ peptide.

3.2. MAGE-A4-specific CD8$^+$ T cells recognize D^d-restricted MAGE-A4$_{265-273}$ peptide

To establish a MAGE-A4 animal model, we determined the minimal epitope of MAGE-A4-specific CD8$^+$ T cells after immunization with MAGE-A4. Naive BALB/c mice were immunized twice at two-week intervals with plasmids encoding the entire sequence of MAGE-A4. Splenic CD8$^+$ T cells were prepared and specific T cell responses were analyzed by ELISPOT assay using peptide pools shown in Supplementary Table 1. MAGE-A4-specific CD8$^+$ T cells were induced in mice immunized with plasmids encoding MAGE-A4 within peptide pool #5 (Fig. 2A). To elucidate the dominant

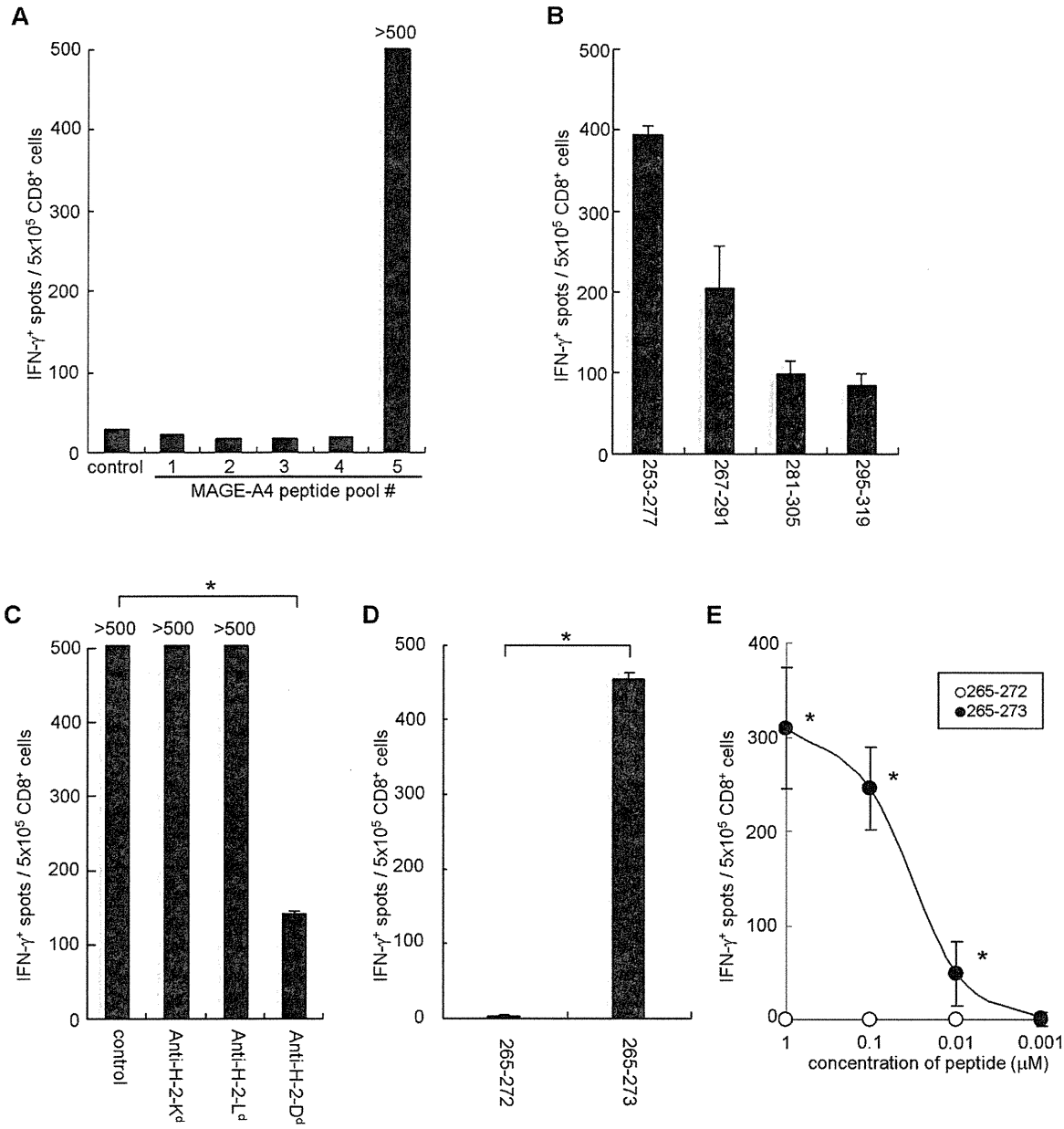

Fig. 2. MAGE-A4-specific CD8$^+$ T cells recognize D^d-restricted MAGE-A4$_{265\text{-}273}$ peptide. (A, B) BALB/c mice were immunized by gene gun twice at two-week intervals with plasmids encoding the entire sequence of MAGE-A4. CD8$^+$ T cells were obtained from spleens, and specific T cells were analyzed with ELISPOT assay using APCs pulsed with the indicated peptides. (C) MHC restriction of induced MAGE-A4-specific CD8$^+$ T cells was analyzed with ELISPOT assay by the addition of the indicated mAb. (D) MAGE-A4$_{253\text{-}277}$ was subjected to BIMAS program and the highest score within MAGE-A4$_{253\text{-}277}$ for a D^d binding motif was predicted in 265–272 and 265–273 of MAGE-A4. These predicted peptides were analyzed with ELISPOT assay for identification of MAGE-A4 epitope peptide. (E) Avidity of MAGE-A4-specific CD8$^+$ T cells was analyzed with ELISPOT assay using APCs pulsed with graded doses of peptides. These experiments were repeated two to four times with similar results. Data are mean ± SD.

MAGE-A4 epitope, MAGE-A4-specific CD8$^+$ T cells were stimulated with each of the peptides from pool #5. The 253–277 peptide was most effective for stimulating MAGE-A4-specific CD8$^+$ T cells (Fig. 2B). We next assessed the restriction of this response using blocking antibodies. MAGE-A4-specific CD8$^+$ T cell responses were completely blocked by anti-H-2 D^d mAb (Fig. 2C). Given the H-2 D^d restriction of this CD8$^+$ T cell response, we employed computer-based BIMAS program to predict optimized MHC class I epitope within the MAGE-A4$_{253\text{-}277}$ peptide. This program ranks all the possible MHC class I epitopes within a given polypeptide sequence. MAGE-A4$_{253\text{-}277}$ was subjected to this program and the highest score within MAGE-A4$_{253\text{-}277}$ for a D^d binding motif was predicted in 265–272 and 265–273 of MAGE-A4 (Supplementary Table 2). MAGE-A4-specific CD8$^+$ T cells recognized the 265–273, but not 265–272 peptides, thus the minimal epitope was considered to be the MAGE-A4$_{265\text{-}273}$ peptide (Fig. 2D). To confirm this minimal epitope, graded doses of peptides were pulsed on APC and specific IFN-γ secretion was analyzed by ELISPOT assay. MAGE-A4-specific CD8$^+$ T cells were high avidity, and could recognize as little as 10 nM of the peptide (Fig. 2E). We conclude that MAGE-A4-specific CD8$^+$ T cells recognize D^d-restricted MAGE-A4$_{265\text{-}273}$ peptide.

3.3. *Kinetics and distribution of NY-ESO-1/MAGE-A4-specific CD8$^+$ T cells after gene gun immunization*

Next, we generated MHC/peptide tetramers based on the data of minimal epitope and MHC restriction for NY-ESO-1/MAGE-A4-specific CD8$^+$ T cells. BALB/c mice were immunized with plasmids

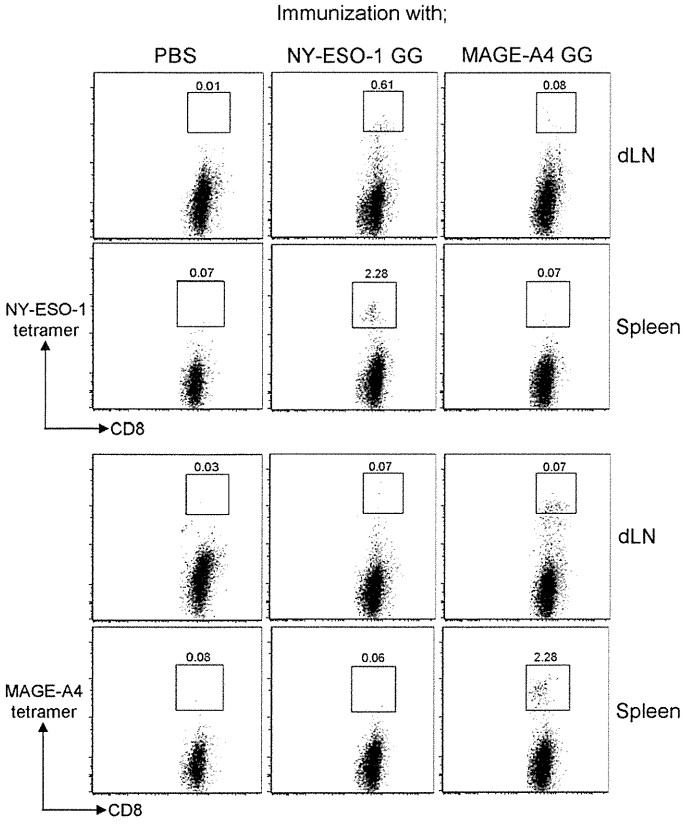

Fig. 3. NY-ESO-1/MAGE-A4-specific CD8$^+$ T cells are detected after immunization with a gene gun. BALB/c mice were immunized twice at two-week intervals with plasmids encoding the entire sequences of NY-ESO-1 or MAGE-A4 using a gene gun. Seven days after the second vaccination, CD8$^+$ T cells were obtained from the draining lymph nodes (dLNs) and spleens, and specific T cells were analyzed with MHC/peptide tetramer assay. These experiments were repeated two to four times with similar results. GG: gene gun.

encoding the whole sequences of NY-ESO-1 or MAGE-A4 by gene gun and the kinetics and distribution of NY-ESO-1/MAGE-A4-specific CD8$^+$ T cells were analyzed with MHC/peptide tetramers. NY-ESO-1-specific CD8$^+$ T cells were detected 7–10 days after the primary immunization both in draining lymph nodes and spleens in mice immunized with plasmids encoding NY-ESO-1, but not in mice immunized with MAGE-A4 or control mice (Fig. 3, 4A and 4B). NY-ESO-1-specific T cell responses were further enhanced by the secondary vaccination in both the draining lymph nodes and spleens (Fig. 4A and B). Similarly, MAGE-A4-specific CD8$^+$ T cells were detected 7–10 days after the primary immunization by gene gun in both the draining lymph nodes and spleens and were enhanced after the booster vaccination (Figs. 3, 4C and 4D), suggesting that these assays are useful tools for analyzing the kinetics and distribution of these antigen-specific CD8$^+$ T cells.

3.4. NY-ESO-1-specific CD8$^+$ T cell responses are primed spontaneously after tumor inoculation and these cells partially inhibit tumor growth

It is important to establish tumor models to re-evaluate cancer immunotherapy strategies in detail. To this end, we employed CT26 (a murine colon carcinoma) tumor transplantation model with stable expression of NY-ESO-1 and examined NY-ESO-1-specific CD8$^+$ T cell and humoral responses spontaneously primed in tumor bearing animals. BALB/c mice were inoculated with CT26-NY-ESO-1 and specific CD8$^+$ T cell and Ab responses were analyzed with MHC/peptide tetramers and ELISA, respectively. NY-ESO-1-specific CD8$^+$ T cells were spontaneously primed 7 days after tumor inoculation in the draining lymph nodes, spleens and peripheral blood in mice inoculated with CT26-NY-ESO-1 and augmented thereafter (Fig. 5A). We then addressed whether these spontaneously-primed NY-ESO-1-specific CD8$^+$ T cells were involved in tumor growth inhibition. To deplete these CD8$^+$ T cells, tumor bearing mice were injected with anti-CD8 mAb and tumor growth was analyzed. Anti-CD8 mAb administration augmented tumor growth compared with the control group without any treatment (Fig. 5C), suggesting an anti-tumor role of spontaneously-primed NY-ESO-1-specific CD8$^+$ T cells. On the other hand, NY-ESO-1-specific Ab responses were not observed 7 days after tumor inoculation, but detected 21 days after tumor inoculation (Fig. 5B). This is compatible with immunological monitoring in humans showing that higher stage of melanoma patients frequently develop humoral immune responses against NY-ESO-1 [3,14].

We next immunized these mice with plasmids encoding the entire sequence of NY-ESO-1 and anti-tumor activity was examined. Tumor growth was significantly reduced by immunization with NY-ESO-1 as compared to the control group without treatment (Fig. 5C). Furthermore, CD8$^+$ T cell depletion totally abolished the anti-tumor effects induced by DNA vaccine (Fig. 5C). As CD4$^+$ regulatory T cells (Tregs) are reportedly associated with spontaneously-primed and treatment-induced anti-tumor immune responses [15], we also investigated tumor-infiltrating Tregs. While Tregs were present in tumors, their frequency was not associated with anti-tumor activity induced by immunization with plasmids encoding NY-ESO-1 (Fig. 5D). Together, CD8$^+$ T cell and Ab responses to NY-ESO-1 in this tumor model closely parallel NY-ESO-1 immune responses in humans. Spontaneous tumor antigen-specific immune responses restrained, albeit incomplete, tumor growth, but tumor growth were vigorous and overwhelmed the tumor growth inhibition, thus additional augmentation of these immune responses are required for effective control of tumor growth.

3.5. MAGE-A4-specific CD8$^+$ T cell responses is primed spontaneously after tumor inoculation

We established another tumor transplantation model with stable expression of MAGE-A4 and examined MAGE-A4-specific CD8$^+$ T cell and humoral responses spontaneously primed in tumor bearing mice. BALB/c mice were inoculated with CT26-MAGE-A4 and specific CD8$^+$ T cell and humoral responses were analyzed with MHC/peptide tetramers and ELISA. In these mice, MAGE-A4-specific CD8$^+$ T cells were spontaneously primed 7 days after tumor inoculation in the draining lymph nodes, spleen and PBMC, and augmented thereafter (Fig. 6A). MAGE-A4-specific Ab responses were not observed 7 days after tumor inoculation, but detected 21 days after tumor inoculation (Fig. 6B). Like as the result of NY-ESO-1 models, cellular and humoral immune responses to MAGE-A4 in this model closely parallel MAGE-A4 immune responses in humans.

4. Discussion

We have established mouse models that allowed studies on NY-ESO-1 and MAGE-A4 immunity. Using these models, we evaluated the kinetics and distribution of antigen-specific CD8$^+$ T cells after tumor growth and immunization. While it has been recently shown that CD4$^+$CD25$^+$ Tregs and the ratio of CD8$^+$ effector T cells to Tregs in tumors critically influenced the prognosis of cancer patients [16,17], limitation of samples usually makes it difficult to investigate the function of effector T cells and Tregs at tumor sites in humans. Given the importance of tumors as active sites of anti-tumor responses, it is important to examine not only the draining

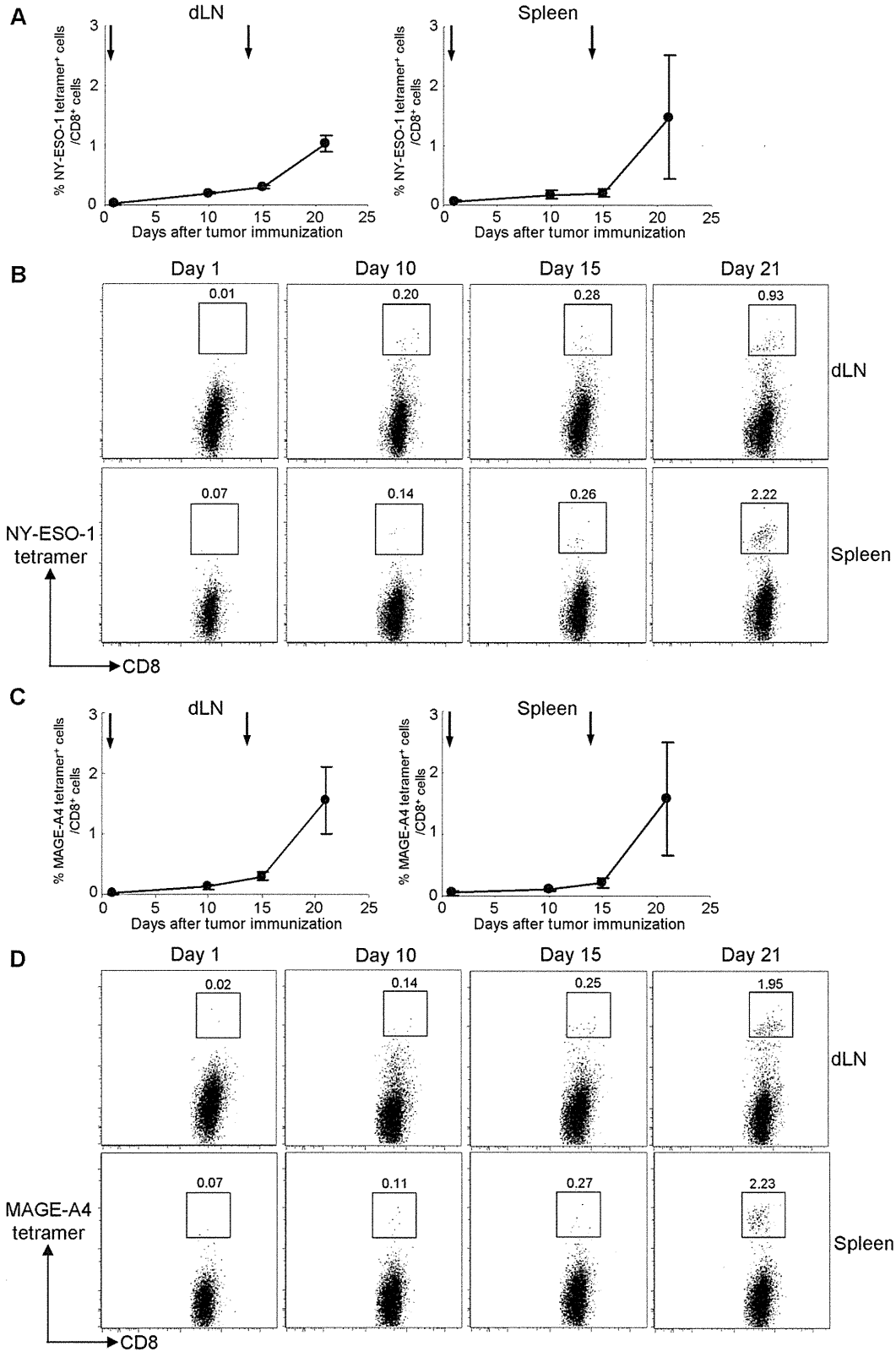

Fig. 4. Kinetics and distribution of NY-ESO-1/MAGE-A4-specific CD8+ T cells after immunization with a gene gun. Kinetics and distribution of NY-ESO-1 (A and B)/MAGE-A4 (C and D)-specific CD8+ T cells were analyzed by MHC/peptide tetramer assay. BALB/c mice were immunized twice at two-week intervals with plasmids encoding the entire sequence of either NY-ESO-1 or MAGE-A4 using a gene gun. CD8+ T cells were obtained from the draining lymph nodes (dLNs) and spleens on the indicated days, and specific T cells was analyzed with MHC/peptide tetramer assay. These experiments were repeated two to four times with similar results. Data in (A) and (C) are mean ± SD. Arrows in (A) and (C) represent the first and second immunization.

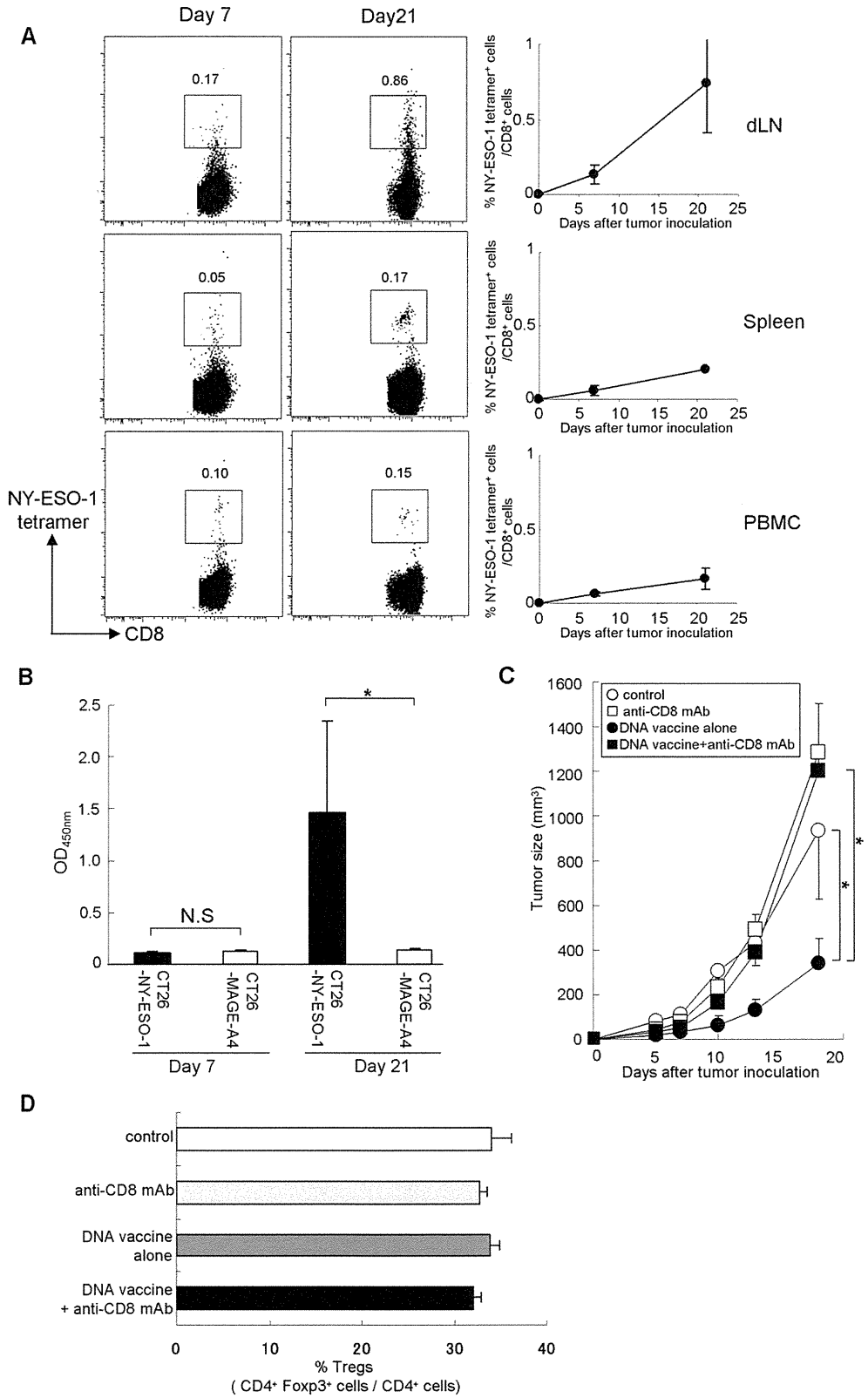

Fig. 5. NY-ESO-1-specific $CD8^+$ T cells are primed spontaneously after tumor inoculation, and these cells partially inhibit tumor growth. BALB/c mice were inoculated with CT26-NY-ESO-1. (A) $CD8^+$ T cells were isolated from the draining lymph nodes (dLNs), spleens and PBMCs on the indicated days, and NY-ESO-1-specific T cells were analyzed with MHC/peptide tetramer assay. (B) Sera were obtained on the indicated days and Ab responses against NY-ESO-1 were analyzed with ELISA. These experiments were repeated twice with similar results. Data are mean ± SD. $^*p < 0.05$ as compared to control. (C) BALB/c mice were immunized with plasmids encoding the entire sequence of NY-ESO-1, and CT26-NYESO-1 was inoculated on day 21 (one week after final immunization). Indicated groups of mice were administered with anti-CD8 mAb (clone 19/178, 100 μg/mouse, every 12 days). More than 95% of $CD8^+$ T cells were depleted by this method (data not shown). Each group consisted of four mice. Mice were monitored thrice a week. These experiments were repeated two times with similar results. (D) Tumor infiltrating lymphocytes were collected 21 days after tumor inoculation and the frequency of $Foxp3^+$ cells in $CD4^+$ T cells was analyzed.

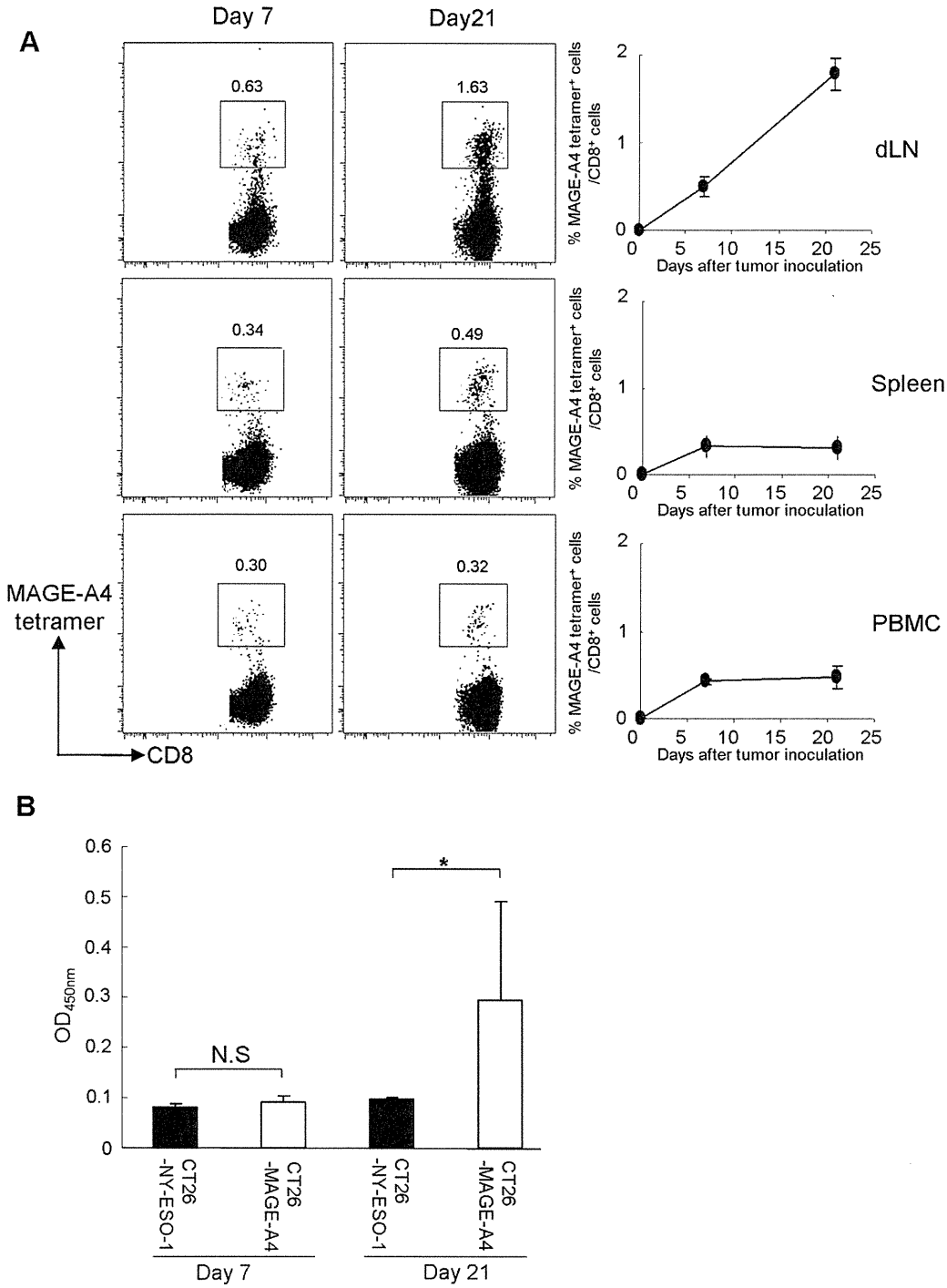

Fig. 6. Spontaneous MAGE-A4-specific $CD8^+$ T cells are primed after tumor inoculation. BALB/c mice were inoculated with CT26-MAGE-A4. (A) $CD8^+$ T cells were isolated from the draining lymph nodes (dLNs), spleens and PBMCs on the indicated days, and MAGE-A4-specific T cells was analyzed with MHC/peptide tetramer assay. (B) Sera were obtained on the indicated days, and Ab responses against MAGE-A4 were analyzed with ELISA. These experiments were repeated twice with similar results. Data are mean ± SD. $^*p < 0.05$ as compared to control.

lymph nodes, spleens and PBMCs, but also tumor local sites. Our models could be valuable tools for analyzing antigen-specific T cells in both novel cancer immunotherapy and cancer immunotherapy that have been already tested in humans.

In our models, we found that spontaneous $CD8^+$ T cell and Ab responses were primed and increased along with tumor progression in both NY-ESO-1 and MAGE-A4 models [3,9]. Accumulating data show that induction/augmentation of anti-tumor immune responses are often detected in patients with larger tumors [3,14], suggesting that immune responses found in our NY-ESO-1 and MAGE-A4 tumor models closely parallel NY-ESO-1 and MAGE-A4 immune responses in humans. It has been a long debate whether spontaneous anti-tumor responses detected in cancer patients impact on tumor growth, as tumors continuously grow in patients harboring spontaneous anti-tumor immune responses. Our tumor model provides a clear answer for this conundrum. Although the immune responses spontaneously primed in tumor-bearing hosts partly inhibit a tumor growth, this immune response